

12-2012

## CHARACTERIZATION OF THE COUNT RATE PERFORMANCE AND EVALUATION OF THE EFFECTS OF HIGH COUNT RATES ON MODERN GAMMA CAMERAS

Michael S. Silosky

Follow this and additional works at: [https://digitalcommons.library.tmc.edu/utgsbs\\_dissertations](https://digitalcommons.library.tmc.edu/utgsbs_dissertations)

 Part of the [Medicine and Health Sciences Commons](#)

### Recommended Citation

Silosky, Michael S., "CHARACTERIZATION OF THE COUNT RATE PERFORMANCE AND EVALUATION OF THE EFFECTS OF HIGH COUNT RATES ON MODERN GAMMA CAMERAS" (2012). *The University of Texas MD Anderson Cancer Center UTHealth Graduate School of Biomedical Sciences Dissertations and Theses (Open Access)*. 304.

[https://digitalcommons.library.tmc.edu/utgsbs\\_dissertations/304](https://digitalcommons.library.tmc.edu/utgsbs_dissertations/304)

This Thesis (MS) is brought to you for free and open access by the The University of Texas MD Anderson Cancer Center UTHealth Graduate School of Biomedical Sciences at DigitalCommons@TMC. It has been accepted for inclusion in The University of Texas MD Anderson Cancer Center UTHealth Graduate School of Biomedical Sciences Dissertations and Theses (Open Access) by an authorized administrator of DigitalCommons@TMC. For more information, please contact [digitalcommons@library.tmc.edu](mailto:digitalcommons@library.tmc.edu).

CHARACTERIZATION OF THE COUNT RATE PERFORMANCE AND EVALUATION  
OF THE EFFECTS OF HIGH COUNT RATES ON MODERN GAMMA CAMERAS

By

Michael Stephen Silosky, B.S.

APPROVED:

---

S. Cheenu Kappadath, Ph. D., Supervisory Professor

---

Charles W. Beasley, Ph. D.

---

William D. Erwin, M.S.

---

Valen E. Johnson, Ph. D.

---

Richard E. Wendt III, Ph. D.

APPROVED:

---

Dean, The University of Texas

Graduate School of Biomedical Sciences at Houston

CHARACTERIZATION OF THE COUNT RATE PERFORMANCE AND EVALUATION  
OF THE EFFECTS OF HIGH COUNT RATES ON MODERN GAMMA CAMERAS

A

THESIS

Presented to the Faculty of  
The University of Texas  
Health Science Center at Houston  
and  
The University of Texas  
M.D. Anderson Cancer Center  
Graduate School of Biomedical Sciences  
In Partial Fulfillment

of the Requirements

for the Degree of

MASTER OF SCIENCE

By

Michael Stephen Silosky, B.S.

Houston, Texas

December 2012

## **Acknowledgements**

I would like to thank my advisor, Dr. Kappadath, for his time and patience in seeing this project to completion. Without his encouragement, I would not have put forth so significant an effort. I also wish to express sincere appreciation to the members of my committee, Drs. Wendt, Beasley, and Johnson and Mr. Erwin for their guidance with this project. Finally, I would want to thank my wife, Joanna, and my children, Hank, Lynne, and Mark for their support and tolerance during what has been a long and often stressful process.

## **Abstract**

### **CHARACTERIZATION OF THE COUNT RATE PERFORMANCE AND EVALUATION OF THE EFFECTS OF HIGH COUNT RATES ON MODERN GAMMA CAMERAS**

Michael Stephen Silosky, B.S.

Supervisory Professor: S. Cheenu Kappadath, Ph.D.

Evaluation of count rate performance (CRP) is an integral component of gamma camera quality assurance and measurement of system dead time ( $\tau$ ) is important for quantitative SPECT. The CRP of three modern gamma cameras was characterized using established methods (Decay and Dual Source) under a variety of experimental conditions. For the Decay method, input count rate was plotted against observed count rate and fit to the paralyzable detector model (PDM) to estimate  $\tau$  (Rates method). A novel expression for observed counts as a function of measurement time interval was derived and the observed counts were fit to this expression to estimate  $\tau$  (Counts method). Correlation and Bland-Altman analysis were performed to assess agreement in estimates of  $\tau$  between methods. The dependencies of  $\tau$  on energy window definition and incident energy spectrum were characterized. The Dual Source method was also used to estimate  $\tau$  and its agreement with the Decay method under identical conditions and the effects of total activity and the ratio of source activities were investigated. Additionally, the effects of count rate on several performance metrics were evaluated. The CRP curves for each system agreed with the PDM at low count rates but deviated substantially at high count rates. Estimates of  $\tau$  for the paralyzable portion of the CRP curves using the Rates and Counts methods were highly correlated ( $r=0.999$ ) but with a small ( $\sim 6\%$ ) difference. No significant difference was

observed between the highly correlated estimates of  $\tau$  using the Decay or Dual Source methods under identical experimental conditions ( $r=0.996$ ). Estimates of  $\tau$  increased as a power-law function with decreasing ratio of counts in the photopeak to the total counts and linearly with decreasing spectral effective energy. Dual Source method estimates of  $\tau$  varied as a quadratic with the ratio of the single source to combined source activities and linearly with total activity used across a large range. Image uniformity, spatial resolution, and energy resolution degraded linearly with count rate and image distorting effects were observed. Guidelines for CRP testing and a possible method for the correction of count rate losses for clinical images have been proposed.

## Table of Contents

1. INTRODUCTION .....	1
Hypothesis and Specific Aims.....	2
2. BACKGROUND .....	3
2.1 Introduction to count rate performance .....	3
2.2 Count rate performance models.....	5
2.3 Count rate performance evaluation.....	8
2.4 Spectral and energy window effects on CRP .....	12
2.5 Modern gamma camera pulse processing.....	13
2.6 Clinical application of CRP correction.....	15
3. SPECIFIC AIM I: DECAY METHOD .....	17
3.1 Objectives .....	17
3.2 Methods .....	18
3.3 Results.....	29
4. SPECIFIC AIM II: DUAL SOURCE METHOD.....	36
4.1 Objectives .....	36
4.2 Methods .....	37
4.3 Results.....	41
5. SPECIFIC AIM III: COMPARISON OF METHODS.....	46
5.1 Objectives .....	46
5.2 Methods .....	47
5.3 Results.....	49
6. SPECIFIC AIM IV: EFFECTS OF HIGH COUNT RATES .....	54
6.1 Objectives .....	54

6.2 Methods .....	55
6.3 Results.....	60
7. DISCUSSION.....	69
7.1 Count rate performance of modern gamma cameras .....	69
7.2 Comparison of the Rates and Counts methods for estimating $\tau$ .....	69
7.3 Specific concerns regarding implementation of the Dual Source method .....	70
7.4 Comparison of the Decay and the Dual Source methods for estimating $\tau$ .....	71
7.5 Comparison and comments on manufacturer specifications .....	72
7.6 Guidelines for CRP testing in a clinical setting.....	73
7.7 Effects of count rate on gamma camera performance metrics .....	74
7.8 Approaches for dead time corrections of SPECT and planar images.....	77
8. CONCLUSION.....	80
9. FUTURE WORK.....	81
10. BIBLIOGRAPHY .....	83
11. APPENDIX: Derivation of the Counts Method model .....	85
12. VITA.....	89



## List of Figures

Figure 2-1	Ideal Count Rate Performance Curves .....	7
Figure 3-1	Rates Method Fitting .....	21
Figure 3-2	Counts Method Fitting .....	24
Figure 3-3	Energy Windows .....	28
Figure 3-4	Modern Gamma Camera Count Rate Performance .....	30
Figure 3-5	Rates Method $\tau$ vs. Counts Method $\tau$ .....	32
Figure 3-6	Rates and Counts Methods Bland-Altman Analysis .....	33
Figure 3-7	Decay Method Energy Window Dependence .....	34
Figure 3-8	Decay Method Effective Energy Dependence .....	35
Figure 4-1	Dual Source Method Source Ratio Dependence .....	42
Figure 4-2	Dual Source Method Count Rate Dependence .....	43
Figure 4-3	Dual Source Method Energy Window Dependence .....	44
Figure 4-4	Dual Source Method Effective Energy Dependence .....	45
Figure 5-1	Decay Method $\tau$ vs. Dual Source Method $\tau$ .....	50
Figure 5-2	Decay and Dual Source Methods Bland-Altman Analysis .....	51
Figure 5-3A	Comparison Energy Window Dependence, Detector 1 .....	52
Figure 5-3B	Comparison Energy Window Dependence, Detector 2 .....	52
Figure 5-4A	Comparison of Effective Energy Dependence, Detector 1 .....	53
Figure 5-4B	Comparison of Effective Energy Dependence, Detector 1 .....	53
Figure 6-1A	Spatial Resolution Test Image .....	57

Figure 6-1B	Truncated Spatial Resolution Test Image .....	57
Figure 6-2A	Edge Response Data .....	57
Figure 6-2B	Derivative of Edge Response Data .....	57
Figure 6-3A	Experimental Setup for Image Distortion Test, Top View .....	59
Figure 6-3B	Experimental Setup for Image Distortion Test, Side View .....	59
Figure 6-4	Image Distortion Region of Interest Placement .....	60
Figure 6-5A	UFOV INT vs. Activity, Paralyzable range .....	61
Figure 6-5B	UFOV DIFF vs. Activity, Paralyzable range.....	61
Figure 6-5C	CFOV INT vs. Activity, Paralyzable range.....	61
Figure 6-5D	CFOV DIFF vs. Activity, Paralyzable range.....	61
Figure 6-6A	UFOV INT vs. Activity, Total range.....	62
Figure 6-6B	UFOV DIFF vs. Activity, Total range.....	62
Figure 6-6C	CFOV INT vs. Activity, Total range.....	62
Figure 6-6D	CFOV DIFF vs. Activity, Total range.....	62
Figure 6-7	Spatial Resolution vs. Activity .....	64
Figure 6-8	Energy Resolution vs. Activity .....	65
Figure 6-9	Photopeak Energy vs. Activity .....	66
Figure 6-10	Center of Mass Location vs. Activity .....	67
Figure 6-11	Percent Maximum Pixel Value vs. Activity .....	67
Figure 6-12	Image Distortion Effects of High Count Rates .....	68

## List of Tables

Table 3-1	Decay Method Sample Data Set.....	19
Table 3-2	Comparison of Rates Method and Counts Method values of $\tau$ .....	25
Table 3-3	Summary of Decay Method Results for Modern Cameras .....	31
Table 5-1	Comparison of Decay Method and Dual Source Method values of $\tau$ .....	47
Table 5-2	Energy Window Dependence Fit Parameters .....	52
Table 5-3	Effective Energy Dependence Fit Parameters .....	53
Table 6-1	Uniformity Analysis Results .....	63

## **List of Abbreviations**

<b>ACR</b>	American College of Radiology
<b>CI</b>	Confidence Interval
<b>CFOV</b>	Central Field of View
<b>CRP</b>	Count Rate Performance
<b>DIFF</b>	Differential Uniformity
<b>FWHM</b>	Full Width at Half Maximum
<b>INT</b>	Integral Uniformity
<b>MCR</b>	Maximum Count Rate
<b>NEMA</b>	National Electrical Manufacturers Association
<b>OW</b>	Open Window
<b>PDM</b>	Paralyzable Detector Model
<b>ROI</b>	Region of Interest
<b>RMS</b>	Root Mean Square
<b>SPECT</b>	Single Photon Emission Computed Tomography
<b>UFOV</b>	Useful Field of View

## 1. INTRODUCTION

Evaluation of count rate performance (CRP) is an integral component of routine quality assurance testing for gamma cameras. Additionally, the American College of Radiology (ACR) requires that count rate performance be evaluated at least annually as part of a nuclear medicine accreditation program.<sup>1</sup> While the National Electrical Manufacturers Association has provided guidelines for CRP testing (Decay method),<sup>2</sup> their suggested procedure requires at least 48 hours of acquisition time, making it cumbersome to perform routinely in a clinical setting. An alternative method for evaluating CRP, commonly referred to as the Dual Source method, has been suggested by Adams *et al.*<sup>3</sup> AAPM Report 6 echoes this recommendation, suggesting that system dead time be evaluated using the Dual Source method under conditions of scatter and at specific count rates<sup>4</sup>. While performance of the Dual Source method is convenient due to short acquisition times, it is valid only for systems that have been demonstrated to follow the paralyzable detector model (PDM). Historically, gamma cameras have been assumed to follow the PDM and several earlier generation gamma cameras were explicitly demonstrated to fit the PDM well. In recent years, advances in hardware and new methods of signal processing have resulted in improved CRP. It has been noted by several authors that a two-component model including paralyzable and non-paralyzable components may more accurately represent the CRP of gamma cameras.<sup>5,6</sup> This work is the first to demonstrate the extent to which the PDM is appropriate for modern gamma cameras. Also, a third method for evaluating CRP requiring the use of attenuating copper sheets to adjust input count rate has been recommended.<sup>7</sup>

In addition to the need for an appropriate method of CRP evaluation as a part of routine quality assurance, an investigation of the CRP of modern gamma cameras can

provide the means of obtaining an important parameter, system dead time ( $\tau$ ). As the interest in quantitative SPECT continues to grow, the ability to correct for count rate losses will become important. To accurately perform SPECT count rate corrections, a thorough understanding of the CRP of modern gamma cameras, including its dependence on the incident energy spectrum and energy window selected, is required.

**The hypothesis upon which the research and results described herein are based, is that the count rate performance of modern Anger type gamma cameras follows the Paralyzable Detector Model only up to a cutoff input count rate, below which the system dead time can be estimated using either the Decay or Dual Source methods.**

The following specific aims by which this hypothesis was tested are:

1. To characterize the count rate performance of modern gamma cameras and to investigate the effects of measurement conditions and acquisition parameters on the evaluation of count rate performance using the Decay Method.
2. To investigate the effects of measurement conditions and acquisition parameters on the evaluation of count rate performance using the Dual Source method.
3. To compare the results of the Decay method and Dual Source method and to identify a technique for evaluating count rate performance that is appropriate for a clinical setting.
4. To investigate the effects of high count rates on gamma camera quality assurance metrics.

## 2. BACKGROUND

### 2.1 Introduction to count rate performance

#### 2.1.1 Gamma camera dead time

Gamma cameras are nuclear counting instruments that are used for medical radionuclide imaging. As with all radiation counting systems, gamma cameras exhibit a characteristic time,  $\tau$ , that is related to the time required to process individual detected events.<sup>8</sup> Following a detected event, there is a discrete amount of time required before a second event can be resolved. When two events occur within this time interval, an overlap of the pulses generated from the detectors occurs. For gamma cameras and other scintillation detectors, this overlap typically results in two effects: pulse pileup and baseline shift.<sup>8</sup> In practice, dead time losses occur in all signal processing components of a counting system. However, counting systems are generally treated as a single unit when evaluating dead time.

#### 2.1.2 Count rate effects: pulse pileup and baseline shift

At high count rates, the events that are detected by a gamma camera may occur in such rapid succession that the voltage pulses generated by the photomultiplier tubes overlap temporally. Two separate effects may result depending on how considerably the pulses overlap. In the case where the overlap is substantial, a single event with a combined pulse height appears to have occurred. This phenomenon is known as pulse pileup, and, as a result, the counting system registers fewer counts than the number of incident gamma rays that actually interacted with the scintillator. While techniques have been developed to reduce the effects of pulse pileup, it remains a significant cause of lost counts at high count rates.<sup>9</sup>

In the case where two events are not close enough in time to “pileup”, but the second pulse is generated while the first pulse still has a substantial voltage, another effect occurs. While both events are registered, the pulse height of the second pulse appears to be different than it properly should be. This phenomenon is known as baseline shift.<sup>9</sup> In gamma cameras, the amplitude of the voltage pulse is proportional to the energy of the detected event. Consequently, baseline shift results in a change in the energy of detected events as count rates increase. A number of techniques have been developed to mitigate baseline shift, and its effect on CRP is not as significant as that of pulse pileup.

### 2.1.3 Energy Discrimination and Count Rate Losses

To create images of sufficient quality to be useful clinically, an important function of a gamma camera is the rejection of events that are the result of background or of scattered radiation. Because the amplitude of the voltage pulse is an indicator of the energy of the incident photon, a pulse-height analyzer is used to selectively count only pulses within a range of amplitudes, i.e., within a range of energies. This process eliminates counts that fall outside of an acceptable energy range.<sup>8</sup> A result of this process is that the effects of pulse pileup are significantly affected by the energy window definition. When two events pile up with no energy discrimination applied, they end up being counted as a single event. However, it is likely that the amplitude of the summed event will correspond to an energy that is outside the acceptable limits. As a result, energy discrimination typically causes the pileup events to be discarded entirely and instead of the loss of a single count, two counts have been lost. It should be noted that, because gamma cameras must process events across a relatively large spectrum before performing energy discrimination, events that fall outside



of the energy window may still have a significant effect on the loss of counts from events that occur within the window.

## 2.2 Count rate performance models

The phenomena described in section 2.1.2 can have a significant effect on the count rates observed using any radiation counting system including gamma cameras. As a result, a counting system may be generally classified as either non-paralyzable, paralyzable, or a combination of paralyzable and non-paralyzable based on their handling of a series of events that occur within a short duration.<sup>8</sup>

### 2.2.1 Non-paralyzable detector model

In the non-paralyzable detector model, events that occur during the interval  $\tau$  following detection are not counted but have no effect on the duration of time the system is “dead”. As a result, the fraction of all time that the detector cannot register an additional count is  $\tau$  multiplied by the observed count rate. Given this, the difference between input and observed count rates may be calculated from the following equation:<sup>9</sup>

Equation 2-1 
$$n - m = nm\tau$$

Where  $n$  is the input count rate and  $m$  is the observed count rate. Solving Eqn. 2-1 for  $n$  results in:

Equation 2-2 
$$n = \frac{m}{1 - m\tau}$$

As a result of this relationship, the observed count rate increases asymptotically toward a maximum value (MCR) where:

Equation 2-3 
$$MCR = \frac{1}{\tau}$$

### 2.2.2 Paralyzable detector model (PDM)

In contrast to the non-paralyzable detector model, a system is referred to as paralyzable when events occurring during the “dead” interval are both uncounted and extend the duration of the interval. As a result, it can be noted that the observed count rate is the rate at which time intervals between events that are greater than  $\tau$  occur. The probability that an event will take place during an incremental time interval ( $dt$ ) that has occurred after a delay of  $\tau$ ,  $P_1(\tau)$  may be given by:<sup>9</sup>

$$\text{Equation 2-4} \quad P_1(\tau)dt = P(0)r dt$$

where  $P(0)$  is the probability that no event will occur between 0 and  $\tau$  and  $r dt$  is the probability of an event occurring during  $dt$ . This is given by the following equation:

$$\text{Equation 2-5} \quad P(0) = \frac{(rt)^0 e^{-rt}}{0!} = e^{-rt}$$

Substitution into Eqn. 2-4 results in:

$$\text{Equation 2-6} \quad P_1(\tau)dt = r e^{-rt} dt$$

Integration of Eqn. 2-6 results in the probability of intervals larger than  $\tau$ . Multiplying this probability by the input count rate results in the following expression for the observed count rate:

$$\text{Equation 2-7} \quad m = n e^{-nt}$$

As a result of this relationship, the observed count rate increases to a maximum value where:

$$\text{Equation 2-8} \quad MCR = \frac{1}{e\tau}$$

Beyond MCR, increases in input count rate result in decreases in observed count rate. At extremely high input count rates, the observed count rate will fall to zero. Eqn. 2-8 indicates that a single parameter, either  $\tau$  or MCR, may be used to describe the CRP of an ideal paralyzable detector. A related quantity, the observed count rate at which 20% of the input

count rate is lost due to count rate effects, is regularly used as a descriptor of count rate performance.

### 2.2.3 Count rate performance curve

As a result of Eqns. 2-2 and 2-7, some substantial differences exist between the paralyzable and non-paralyzable detector models. Fig. 2-1 illustrates these differences by plotting observed count rate against input count rate (CRP curve). The CRP curve is a useful tool for evaluating count rate losses over a range of input count rates.

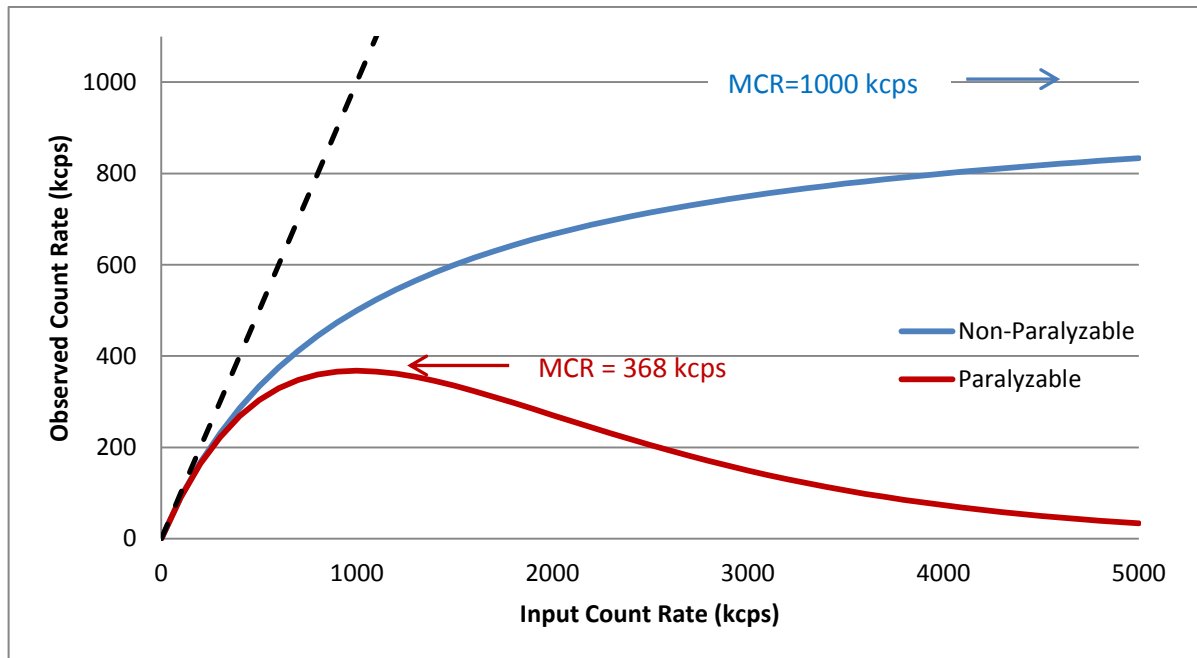


Fig.2-1. The observed count rate plotted against input count rate for both the paralyzable and non-paralyzable detector models for  $\tau = 1\mu\text{s}$ . The dashes indicate the line where there are no count rate losses. Substantial differences in both the shape of the CRP curves and the MCR between models are clearly visible.

#### 2.2.4 Combined paralyzable/non-paralyzable systems

While the models presented in sections 2.2.1 and 2.2.2 represent ideal paralyzable and non-paralyzable systems respectively, it has been suggested that gamma cameras are likely to have both paralyzable and non-paralyzable components. If so, the CRP curves for these systems would result from a combination of these models. It has been demonstrated that at least some gamma cameras behave in this fashion, though the investigator acknowledges that his results have been disputed by other authors.<sup>5</sup> Adams *et al.* demonstrated that a number of historical gamma cameras simply followed the PDM<sup>3</sup>. Theoretical models for the behavior of combined systems have been suggested with the shape of the CRP curve strongly dependent on the values of  $\tau$  for the paralyzable and non-paralyzable components<sup>6</sup>.

### 2.3 Count rate performance evaluation

#### 2.3.1 Decay method

The Decay method for evaluating CRP consists of exposing an uncollimated detector to a radioactive source (typically Tc-99m) that initially produces substantial count rate loss due to dead time, and then sampling the count rate at intervals over a period of time sufficient such that radioactive decay of the source results in input count rates below those that would lead to significant count loss. For a paralyzable detector, the initial activity of the source is selected such that the initial input count rate is greater than what is required to reach the MCR. Background measurements are performed before and after this acquisition and used to correct the observed count rates. On the basis of the assumption that count rate losses are negligible at the measured low count rates, the background-corrected lowest count

rates can be considered equivalent to the input count rate. The input count rates corresponding to all other observed count rates may be estimated by scaling the lowest count rate by the relative decay in activity due to the difference in time in accordance with the following equation:<sup>2</sup>

Equation 2-9 
$$n_i = m_n e^{\lambda(t_n - t_i)}$$

where  $n_i$  is the input count rate for data point  $i$ ,  $m_n$  is the background corrected observed count rate for the last data point,  $\lambda$  is the decay constant of the radioactive source, and  $t_i$  and  $t_n$  are the relative times at which measurements for data points  $i$  and  $n$ , respectively were made. Two important points should be noted in regards to this procedure. First, count rate losses are assumed to be negligible for the measurements of the background and the lowest observed count rates. Second, low count rate data points are particularly sensitive to the magnitude of the background corrections. For these reasons, care must be taken to ensure that data are acquired under low and stable background conditions and that the last data point occurs at a sufficiently low count rate.

With the input count rate and observed count rate known for each data point, the CRP curve may be plotted and the MCR and observed count rate at 20% loss may be derived. For an ideal paralyzable system,  $\tau$  may be calculated from this MCR using Eqn. 2-3. In practice, it has been demonstrated that while some gamma cameras agree with the PDM,  $\tau$  estimated from the MCR in this fashion can vary substantially<sup>10</sup>. In this work estimation of  $\tau$  from decay data involved either fitting the PDM to the set of input and output count rates (Rates method) or fitting an expression derived from the PDM for the observed

counts (Counts method) in each counting interval via non-linear least squares regression. These methods will be discussed further in the Materials and Methods section of Specific Aim I. The advantage of the Decay method is that the entire CRP curve, including the MCR (which is the most common metric quoted by vendors) is directly measured. The disadvantage is that the Decay method requires long acquisition times while maintaining a relatively constant background and the use of curve fitting software to estimate  $\tau$ .

### 2.3.2 Dual Source method

The Dual Source method for evaluating CRP involves making three count-rate measurements using two sources of similar activity, with the detector exposed to each source individually as well as to both concurrently. As with the Decay method, these measurements must be corrected for background. Once these measurements are made,  $\tau$  may be estimated based on the following equation:<sup>3</sup>

Equation 2-10 
$$\tau = \frac{2R_{12}}{(R_1 + R_2)^2} \ln\left(\frac{R_1 + R_2}{R_{12}}\right)$$

where  $R_1$  and  $R_2$  are the background corrected observed count rates for source 1 and source 2, respectively and  $R_{12}$  is the background corrected observed count rate for sources 1 and 2 concurrently. Eqn. 2-10 may be derived directly from Eqn. 2-7 under the assumption that sources 1 and 2 are equal in activity and produce similar observed count rates. Eqn. 2-7 may be rewritten as

Equation 2-11 
$$n = me^{n\tau}$$

For a detector exposed to two sources of equal activity the input count rate can be written as

Equation 2-12 
$$n_{12} = n_1 + n_2$$

where  $n_{12}$ ,  $n_1$ , and  $n_2$ , are the input count rates for both sources simultaneously, source 1 alone, and source 2 alone, respectively. Substitution of Eqn. 2-11 into Eqn. 2-12 results in the following expression

Equation 2-13 
$$m_{12}e^{n_{12}\tau} = m_1e^{n_1\tau} + m_2e^{n_2\tau}$$

where  $m_{12}$ ,  $m_1$ , and  $m_2$ , are the observed count rates for both sources simultaneously, source 1 alone, and source 2 alone, respectively. Assuming  $n_1 = n_2 = n^*$  and  $m_1 = m_2 = m^*$ , Eqn. 2-13 may be simplified as follows:

Equation 2-14 
$$m_{12}e^{2n^*\tau} = 2m^*e^{n^*\tau}$$

which can be rewritten as

Equation 2-15 
$$e^{n^*\tau} = \frac{2m^*}{m_{12}}$$

Eqn. 2-15 may be solved for  $\tau$  resulting in the following expression

Equation 2-16 
$$\tau = \frac{1}{n^*} \ln\left(\frac{2m^*}{m_{12}}\right)$$

which can be further simplified by substitution of Eqn. 2-11 for  $n^*$  to yield

Equation 2-17 
$$\tau = \frac{m_{12}}{2(m^*)^2} \ln\left(\frac{2m^*}{m_{12}}\right)$$

The final form of this expression (Eqn. 2-10) replaces  $m_{12}$  and  $m^*$  with the background corrected observed rates  $R_{12}$  and  $\frac{R_1+R_2}{2}$  respectively. The advantage of the Dual Source method is that  $\tau$  may be estimated algebraically, with data acquisition occurring over a relatively short interval (< 10 minutes) and without the use of curve fitting software. The

disadvantages are that the gamma camera in question must follow the PDM for Eqn. 2-10 to be valid and that the MCR is never measured directly.

### 2.3.3 Attenuation method

The Attenuation method for evaluating CRP involves exposing a detector to a relatively high activity source and making a series of count rate measurements where the input count rate is adjusted by adding layers of copper to attenuate the intensity of the radiation incident on the detector. Several procedures have been recommended regarding the implementation of this method.<sup>7,11</sup> The Attenuation method ultimately generates a CRP curve that is more sparsely sampled than what is possible using the Decay method, and it is labor intensive to perform. Additionally, due to the exponential behavior of attenuation, the density of data points at higher count rates is less than at lower count rates. This makes direct measurement of MCR difficult using the Attenuation method. For these reasons, the Attenuation method was not used in this work.

## 2.4 Spectral and energy window effects on CRP

### 2.4.1 Energy Window Definition and Incident Energy Spectrum

As described in section 2.1.3, the energy window definition can have a significant effect on count rate losses. These losses are the result of the count rate across the entire energy spectrum and are not limited to the range of energies that are accepted by the energy window used for imaging. Consequently, the ratio of counts in the photopeak window to the counts across the entire spectrum is important when considering count rate losses. It should be noted that this ratio is dependent on both the energy window definition and the incident energy spectrum. Preliminary observations of clinical studies indicate that this ratio may



vary significantly depending on the number and widths of the energy windows used. While this ratio is likely to play a significant role in the effects of count rate losses, the nature of these effects remains to be determined.

#### 2.4.2 Incident Spectral Energy

As stated in section 2.1.2, the amplitude of the voltage pulse generated from a single event is used to determine the energy of an incident photon. Historically, system dead time has been assumed to be relatively independent of the energy of the incident event. As a result, the differences in count rate loss due to variations in the incident spectrum have been attributed to the effects of energy discrimination. It is possible, however, that the system dead time varies with the energy of the incident photon. In this case, the ratio of counts in the photopeak window to the total counts would be only one contributing factor to count rate losses. Therefore, to fully characterize the CRP of a gamma camera, it is important to investigate the dependence of count rate losses on the energy of the incident spectrum, independent of the effects of energy discrimination. To identify this dependence, CRP can be evaluated using an open energy window (OW) that captures counts across the entire spectrum.

### 2.5 Modern gamma camera pulse processing

#### 2.5.1 Tail fitting

In traditional gamma cameras, following an interaction, the signal generated by individual photomultiplier tubes (PMT) would be amplified and summed before being sent to a pulse height analyzer. In some modern gamma cameras, voltage pulses generated from individual PMTs are digitized following amplification. Instead of summing, the digitized

signals are each individually sent to a digital event processor. Normally, to obtain the complete signal from an event, the voltage pulse must be integrated over its entire length. In the case where any individual PMT experiences high count rates and pulse pileup may occur, some modern cameras will halt the integration of the first pulse, calculate the remaining tail based on the known pulse shape, add this remaining signal to the first pulse, and subtract it from the second. Such pileup correction algorithms lead to a reduction in  $\tau$ , since less time is required between individual events.

### 2.5.2 Multi-zone architecture

Another method that has been suggested to minimize the effects of high count rates is the use of multiple geographic zones detection. In a traditional gamma camera, signals that occur within a short enough period of time will be summed regardless of their PMT of origin. In this case, signals from PMTs that are not spatially close will still be summed, even though it is not possible for these signals to have arisen from a single event. To avoid this, it has been suggested that detectors could be designed to avoid pileup by summing signals that occur not only within a timing window but also originate from nearby PMTs. It has been suggested that such a detector could reduce dead time losses in proportion to the number of zones used<sup>6</sup>. As such, a five-zone detector would increase the MCR of the system by five, with the corresponding reduction in overall dead time.

## **2.6 Clinical Application of CRP correction**

Based on observations of clinical exams, common Nuclear Medicine imaging procedures rarely exceed 20 kcps in the particular photopeak energy window used. In fact, clinical count rates are often below 10 kcps. Preliminary investigation of observed count rates for eight Tc-99m bone scan studies found that, on average, the observed count rate in the photopeak window was approximately 5 kcps, with no studies exceeding 10 kcps. However, it is important to note that counts in the photopeak window only represent a fraction of the total counts across the entire spectrum. Based on spectra captured from these bone scan patients, counts in the photopeak window represent approximately 27% of the total counts across the spectrum on average. A similar ratio of counts in the photopeak window to counts across the entire spectrum was observed for several other diagnostic procedures. As a result, the total count rates may be closer to 40 kcps on average and approach 80 kcps in certain cases. Further investigation is required to verify these observations and the significance of dead time effects at these count rates remains to be determined.

While diagnostic Nuclear Medicine procedures may produce relatively low count rates, it has been demonstrated that several radionuclide therapy procedures result in significantly higher count rates during post therapy imaging. Because of the large administered activity for these procedures and the high count rates that are a direct result, post therapy imaging often occurs after a period of time sufficient to allow for both physical and biological decay. If correction for count rate losses could be applied to clinical images, it might be possible to perform post-therapy imaging more promptly after administration. Additionally, it is generally assumed that for radionuclide therapy patients, the distribution

of activity within the patient is the same for low as well as high activities. The ability to correct for count rate losses for high activity images will allow for the assessment of the validity of this assumption. One purpose of this work is to lay some groundwork for count rate loss correction for clinical studies.

### 3. SPECIFIC AIM I

To characterize the count rate performance of modern gamma cameras and to investigate the effects of measurement conditions and acquisition parameters on the evaluation of count rate performance using the Decay method.

#### 3.1 Objectives for Specific Aim I

To characterize the CRP of modern cameras, it is necessary to determine what portion, if any, of the CRP curve is characterized by the PDM and if so, what parameters affect the estimation of  $\tau$  in this region. To perform these investigations, a thorough understanding of the methods of analyzing CRP data and their results is necessary. To achieve Specific Aim I, the following five objectives were investigated:

**3.1.1 Objective 1:** Determine if all or a portion of the CRP curve for modern gamma cameras follows the PDM.

**3.1.2 Objective 2:** Evaluate the precision in  $\tau$ , estimated using the Decay method, for the paralyzable portion of the CRP curve.

**3.1.3 Objective 3:** Determine if  $\tau$ , estimated using the Rates fitting method provides the same result as  $\tau$  estimated using the Counts fitting method.

**3.1.4 Objective 4:** Identify the dependence of  $\tau$  on the energy window selected when estimated using the Decay method.

**3.1.5 Objective 5:** Identify the dependence of  $\tau$  on the incident energy spectrum when estimated using the Decay method and an open energy window.

## **3.2 Methods for Specific Aim I**

### **3.2.1 Method for Specific Aim I, Objective 1**

#### **3.2.1.1 Method of data acquisition for Specific Aim I, Objective 1**

To determine if all or a portion of the CRP of modern gamma cameras follows the PDM, the Decay method was performed to measure the CRP curve for both detectors on a Symbia (Siemens Medical Systems), a Brightview (Philips Medical Systems), and a Millennium (General Electric Healthcare) gamma camera. The uncollimated detectors were exposed to a Tc-99m source and counts were acquired for sequential counting intervals over a 48 hour period. For the Symbia and Brightview cameras, counting intervals were 2 minutes for the first 12 hours, followed by 4, 8 and 16 minute intervals for each subsequent 12 hour period. For the Millennium, the first two 12 hour periods were composed of 2 and 4 minute intervals respectively, followed by 24 hours of 16 minute intervals. The Symbia was evaluated with the source placed in a syringe free-in-air (AIR) and using an open energy window (OW) intended to capture counts across the entire spectrum. The OW was composed of the following adjacent energy windows: 17.5-52.5 keV, 52.5-157.5 keV, 157.5-472.5 keV, and 472.5-687.3 keV. Additionally, the Symbia was evaluated with the source placed in a lead shield with an opening covered by 6 mm of copper plates (NEMA)

and using the manufacturer's 15% photopeak window in accordance with NEMA NU1-2007. The Brightview was evaluated using the AIR scatter condition and an OW. The Millennium was evaluated using the NEMA scatter condition and the manufacturers 20% photopeak window. Ten-minute background measurements were made before and after data acquisition. Input count rates were estimated based on the lowest count rate data point. The resulting data for each detector were evaluated using two methods (Rates and Counts) to determine if all or a portion of the CRP curve followed the PDM and to estimate the value of  $\tau$  for this portion. Table 3-1 provides some sample data from the first 15 time points for a single detector to illustrate the results of the decay measurements.

Table 3-1. Counts observed during the first 15 time intervals of a Decay acquisition performed on a Symbia gamma camera are tabulated as well as the interval duration, mean time from the beginning of the experiment, the relative activity for the interval in question, and the corresponding count rates. Observed count rates increase as the source decays because the input count rate is beyond that which results in the maximum observed count rate.

<b>Observed Counts</b>	<b>Duration (min)</b>	<b>Mean Time (min)</b>	<b>Relative Act</b>	<b>Observed Count Rate (kcps)</b>	<b>Bg. Corrected Observed Count Rate (kcps)</b>	<b>Input Count Rate (kcps)</b>
38269808	2	1	0.996	318.92	318.29	870.76
38289812	2	3	0.992	319.08	318.46	867.42
38314514	2	5	0.989	319.29	318.66	864.09
38342385	2	7	0.985	319.52	318.89	860.77
38367808	2	9	0.981	319.73	319.11	857.47
38383853	2	11	0.977	319.87	319.24	854.18
38409864	2	13	0.973	320.08	319.46	850.90
38430252	2	15	0.970	320.25	319.63	847.63
38460536	2	17	0.966	320.50	319.88	844.38
38486651	2	19	0.962	320.72	320.10	841.14
38513174	2	21	0.959	320.94	320.32	837.91
38547069	2	23	0.955	321.23	320.60	834.69
38572294	2	25	0.951	321.44	320.81	831.49
38602409	2	27	0.948	321.69	321.06	828.30
38634311	2	29	0.944	321.95	321.33	825.12

### 3.2.1.2 Method of data analysis for Specific Aim I, Objective 1

#### Rates Method Procedure

The Rates method for evaluating the results of Decay method measurements involves fitting the observed and input count rates to the PDM (Eqn. 2-7) via non-linear least squares regression. The observed count rates were calculated for each data point and the input count rates were estimated based on Eqn. 2-9, modified to account for the effects of inter-frame decay resulting from different counting interval durations as follows:

Equation 3-1 
$$n_i = m_n e^{\lambda(t_n - t_i)} \frac{(\Delta t_n - \Delta t_n e^{(-\lambda \Delta t_i)})}{(\Delta t_i - \Delta t_i e^{(-\lambda \Delta t_n)})}$$

where  $\Delta t_n$  and  $\Delta t_i$  are the durations of counting intervals  $n$  and  $i$ , respectively. To evaluate the quality of the fit, the Root Mean Square (RMS) of the residuals (fit-measurement) was calculated. Visual inspection of CRP data (Fig. 3-1) indicates that only a portion of the CRP curve followed the PDM. To identify the input count rate at which the CRP curve begins to deviate from the PDM, data points were removed one by one from the high count rate end of the curve and the fit was repeated. A threshold of less than 2% for RMS residuals was chosen to indicate that the fitted CRP data were adequately described by the PDM. Additionally, the percentage change in RMS residuals was calculated for each consecutive data point removed from the fit range. Small changes in RMS residuals imply that the change in the fit (and consequently the model parameters) is not substantial, i.e., the value of  $\tau$ , derived from the fit is relatively stable. Under this reasoning,  $\tau$  in this work was determined from the fit of measured CRP data to be the value where the RMS residuals were



below 2% and where RMS residuals changed by less than 1% from the previous fit (that included one additional CRP measurement).

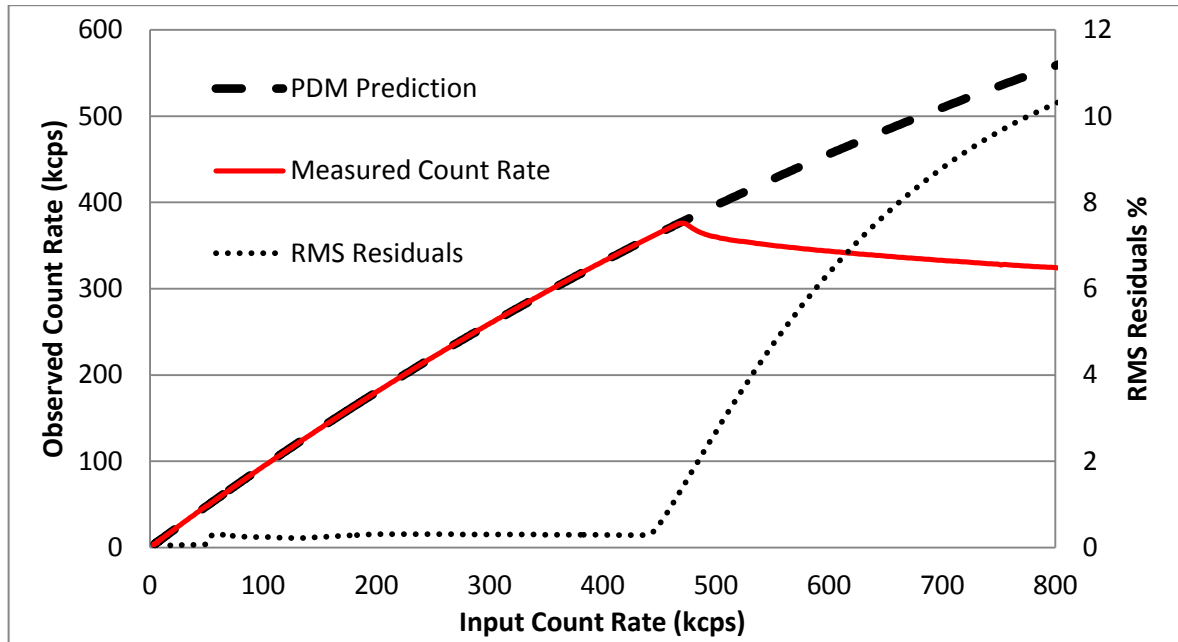


Fig. 3-1. The measured CRP curve for a Symbia detector acquired using a Tc-99m source (AIR) and an open energy window is plotted along with the ideal CRP behavior predicted by the PDM. For this detector, the observed CRP appears to agree well with the PDM prediction up to a certain observed count rate of 375 kcps, beyond which the observed count rate deviates dramatically. The RMS residuals calculated for least-squares fits of the observed count rates up to a maximum input count rate to the PDM are shown plotted against the maximum input count rate included in the fit. The quality of the fit improves and RMS residuals decreases as the maximum input count rate included in the fit decreases. When the fitted observed count rate data range lies along the paralyzable portion of the CRP curve, the RMS residuals cease to decrease and the quality of the fit remain relatively constant.

Although the Rates method is a relatively straightforward procedure for estimating  $\tau$  from Decay method data, two important points should be noted in regards to this procedure. First, it does not account for the fact that the background count rate is affected by count rate loss itself when the observed count rate is corrected for background. When background is estimated, the count rate is typically low, and so there is little loss. At higher count rates, the background count rate, as a constituent of the overall count rate, will experience some

loss, resulting in an over correction of the observed count rate. Second, because the Rates method estimates the input count rate for each data point based on the lowest observed count rate data point, statistical fluctuations may lead to errors that are propagated throughout the entire data set. This disadvantage may be mitigated by utilizing a sufficiently long counting interval so that the uncertainty in the lowest observed count rate is small.

### Counts Method Procedure

For the reasons stated above, an additional procedure was developed (Counts method) for analyzing Decay method data. An expression was derived from the PDM for the counts observed during a counting interval from  $t_0$  to  $t_1$ , assuming that the background count rate was subject to count rate losses and that the input count rate was subject to radioactive decay. In this case, the input count rate can be expressed as:

$$\text{Equation 3-2} \quad n(t) = b + A_0 e^{-\lambda(t-t_0)}$$

where  $b$  is the background count rate,  $A_0$  is the portion of the input count rate that is due entirely to the decay of the source at time 0,  $\lambda$  is the decay constant for the source in question, and  $t$  is the time since  $t_0$ . Substituting Eqn. 3-2 for  $n$  in Eqn. 2-7 and integrating over a time interval ( $t_0$  to  $t_1$ ) results in an expression for the counts observed during that interval,  $M(t_0, t_1)$  that accounts for losses to the background.

$$\text{Equation 3-3} \quad M_{(t_0, t_1)} = b e^{-b\tau} \int_{t_0}^{t_1} e^{-(A_0 e^{-\lambda t})\tau} dt + \frac{e^{-b\tau}}{\lambda\tau} (e^{-(A_0 \tau e^{-\lambda t_1})} - e^{-(A_0 \tau e^{-\lambda t_0})})$$

As shown in the appendix, the solution to Eqn. 3-2 can be written as

$$\begin{aligned} \text{Equation 3-4} \quad M_{(t_0, t_1)} &= \frac{e^{-b\tau}}{\lambda\tau} \left( e^{-(A_0\tau e^{-\lambda t_1})} - e^{-(A_0\tau e^{-\lambda t_0})} \right) + b e^{-b\tau} (t_1 - t_0) \\ &+ \frac{A_0\tau}{\lambda} b e^{-b\tau} \left( e^{-\lambda t_1} - e^{-\lambda t_0} \right) \left( 1 - \frac{A_0\tau}{2} e^{-\frac{\lambda(t_1+t_0)}{2}} + \frac{(A_0\tau)^2}{6} e^{-\lambda(t_1+t_0)} - \frac{(A_0\tau)^3}{24} e^{-\frac{3\lambda(t_1+t_0)}{2}} \right) \end{aligned}$$

The counts measured over known time intervals (Fig. 3-2) using the Decay method can be modeled using Eqn. 3-4 to estimate  $\tau$ ,  $b$ , and  $A_0$ . As with the Rates method, the Counts method was used to fit the Decay data and the RMS residuals were calculated. This fit and RMS calculation were repeated as data points were removed from the high count rate end of the CRP curve. The percentage change in RMS residuals from the previous data point was calculated. As with the Rates method, a threshold of less than 2% for RMS residuals was chosen to indicate that the fitted CRP data were adequately described by the PDM and the model parameters ( $\tau$ ,  $b$ , and  $A_0$ ) were determined at the data point where RMS residuals changed by less than 1% from the previous fit.

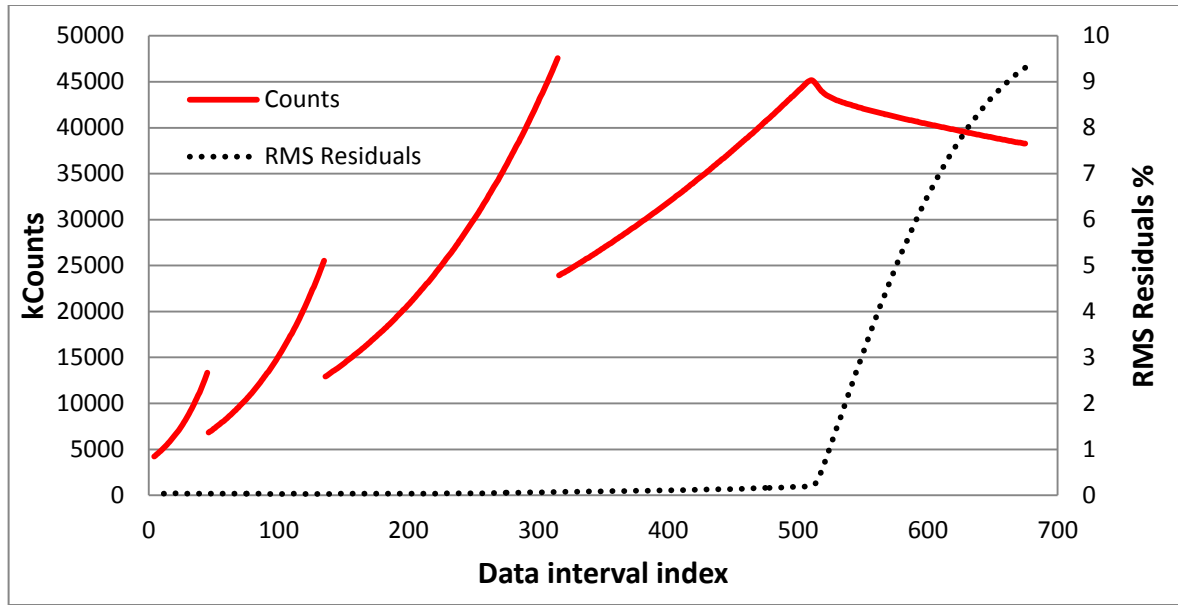


Fig. 3-2. The observed counts at each counting interval plotted against the data interval index for a Symbia 3/8 in. crystal detector. Discontinuities in the observed counts (at index values of 45, 135, and 316) are the result of doubling the counting interval duration every twelve hours to help maintain uniform counting statistics. The observed discontinuity at the index value of 508 is due to the deviation of the measured count rate from the PDM. The RMS residuals calculated for least-squares fits of the observed counts using Eqn. 3-4 are shown plotted against the maximum data interval included in the fit. As with the Rates method, as high count rate data points are removed from the fit, its quality improves and the RMS residuals decrease. When the fitted observed count data lie along the paralyzable portion of the CRP curve, the RMS residuals cease to decrease and the fit quality remains relatively constant.

### 3.2.2 Method for Specific Aim I, Objective 2

#### 3.2.2.1 Method of data acquisition for Specific Aim I, Objective 2

To evaluate the precision in  $\tau$  estimated using both the Rates and Counts methods, decay measurements were performed five times on the same Symbia system using the AIR scatter condition and OW.

### 3.2.2.2 Method of data analysis for Specific Aim I, Objective 2

The mean value of  $\tau$  ( $\tau_m$ ), and the standard deviation ( $\sigma$ ) and fractional error in  $\tau$  were calculated, where:

Equation 3-5 
$$\text{Fractional Error (\%)} = \sigma / \tau_m \times 100$$

### 3.2.3 Method for Specific Aim I, Objective 3

#### 3.2.3.1 Method of data acquisition for Specific Aim I, Objective 3

To assess agreement between the Rates and Counts methods, the Decay Method was performed for 42 combinations of gamma cameras detector, energy windows, and spectral conditions using both methods shown in Table 3-2.

Table 3-2.  $\tau$  estimated for the paralyzable portion of the CRP curve using both the Rates and Counts methods is tabulated with their difference and mean value for 42 combinations of camera, detector, incident spectrum and energy window width.

Camera	Detector	Scatter Cond.	Energy Window	Rates Tau ( $\mu$ s)	Counts Tau ( $\mu$ s)	Difference ( $\mu$ s)	mean ( $\mu$ s)
Symbia S1	1	AIR	OW	0.389	0.373	0.016	0.381
Symbia S1	1	NEMA	15% PW	0.896	0.894	0.002	0.895
Symbia S1	2	AIR	OW	0.394	0.390	0.004	0.392
Symbia S1	2	NEMA	15% PW	1.110	1.120	-0.010	1.115
Symbia S2	1	AIR	OW	0.439	0.410	0.029	0.425
Symbia S2	1	AIR	OW	0.437	0.404	0.033	0.421
Symbia S2	1	AIR	OW	0.445	0.409	0.036	0.427
Symbia S2	1	AIR	OW	0.443	0.410	0.033	0.427
Symbia S2	1	AIR	OW	0.442	0.409	0.033	0.426
Symbia S2	1	AIR	15% PW	1.120	1.120	0.000	1.120
Symbia S2	1	NEMA	OW	0.430	0.402	0.028	0.416
Symbia S2	1	NEMA	15% PW	0.840	0.986	-0.146	0.913
Symbia S2	1	Scatter Block	OW	0.481	0.450	0.031	0.466
Symbia S2	1	Scatter Block	15% PW	2.170	2.130	0.040	2.150
Symbia S2	1	Sc. Bl. + Acrylic	OW	0.507	0.476	0.031	0.492
Symbia S2	1	Sc.Bl.+Acr.+Pb	OW	0.509	0.509	0.000	0.509

Symbia S2	1	AIR	2% PW	7.820	7.690	0.130	7.755
Symbia S2	1	AIR	6% PW	2.800	2.670	0.130	2.735
Symbia S2	1	AIR	75% PW	0.512	0.495	0.017	0.504
Symbia S2	2	AIR	OW	0.405	0.376	0.029	0.391
Symbia S2	2	AIR	OW	0.411	0.376	0.035	0.394
Symbia S2	2	AIR	OW	0.419	0.378	0.041	0.399
Symbia S2	2	AIR	OW	0.413	0.378	0.035	0.396
Symbia S2	2	AIR	OW	0.412	0.378	0.034	0.395
Symbia S2	2	AIR	PW	1.230	1.220	0.010	1.225
Symbia S2	2	NEMA	OW	0.398	0.364	0.034	0.381
Symbia S2	2	NEMA	15% PW	0.987	0.963	0.024	0.975
Symbia S2	2	Scatter Block	OW	0.448	0.414	0.034	0.431
Symbia S2	2	Scatter Block	15% PW	2.450	2.390	0.060	2.420
Symbia S2	2	Sc. Bl. + Acrylic	OW	0.469	0.437	0.032	0.453
Symbia S2	2	Sc.Bl.+Acr.+ Pb	OW	0.482	0.465	0.017	0.474
Symbia S2	2	AIR	2% PW	9.090	8.930	0.160	9.010
Symbia S2	2	AIR	6% PW	3.400	3.300	0.100	3.350
Symbia S2	2	AIR	75% PW	0.506	0.495	0.011	0.501
Symbia S4	1	AIR	OW	0.451	0.409	0.042	0.430
Symbia S4	2	AIR	OW	0.410	0.371	0.039	0.391
Symbia T4	1	AIR	OW	0.498	0.455	0.043	0.477
Symbia T4	2	AIR	OW	0.887	0.859	0.028	0.873
Brightview	1	AIR	OW	0.859	0.837	0.022	0.848
Brightview	1	AIR	OW	0.857	0.967	-0.110	0.912
Millennium	1	NEMA	20% PW	0.909	0.900	0.009	0.905
Millennium	2	NEMA	20% PW	0.956	0.906	0.050	0.931

### 3.2.3.2 Method of data analysis for Specific Aim I, Objective 3

The mean difference in  $\tau$ , standard deviation of the differences, and the standard error in the mean difference were calculated. A paired t-test was performed to evaluate the magnitude and significance of the mean difference. The degree of correlation between the two methods was evaluated by calculating the Pearson product-moment correlation coefficient ( $r$ ). Additionally, a Bland-Altman<sup>12</sup> analysis was performed to characterize the correlation between methods and to evaluate potential biases.

### **3.2.4 Method for Specific Aim I, Objective 4**

#### **3.2.4.1 Method of data acquisition for Specific Aim I, Objective 4**

To evaluate the effect of the energy window definition on estimates of  $\tau$ , the Decay method was performed five times on both detectors of a Symbia gamma camera, using different photopeak window widths of 2%, 6%, 15%, 75%, and an OW, with a Tc-99m point source, and the AIR scatter condition. A spectrum was acquired on each detector with a source of sufficient activity such that the observed count rate was approximately 95% of the MCR.

#### **3.2.4.2 Method of data analysis for Specific Aim I, Objective 4**

For the paralyzable portion of the CRP curves,  $\tau$  was determined for all detectors using both the Rates and Counts methods. The energy spectrum was used to determine the ratio of counts in each photopeak window to the total counts (Fig. 3-3). The range in  $\tau$  for the energy windows used was determined. The functional form of the dependence of  $\tau$  on the ratio of photopeak window counts to open window counts was determined. An estimate of  $\tau$ , for a 20% photopeak window, was computed from the functional form, and the difference in  $\tau$  between the measured 15% window and the computed 20% window was calculated.

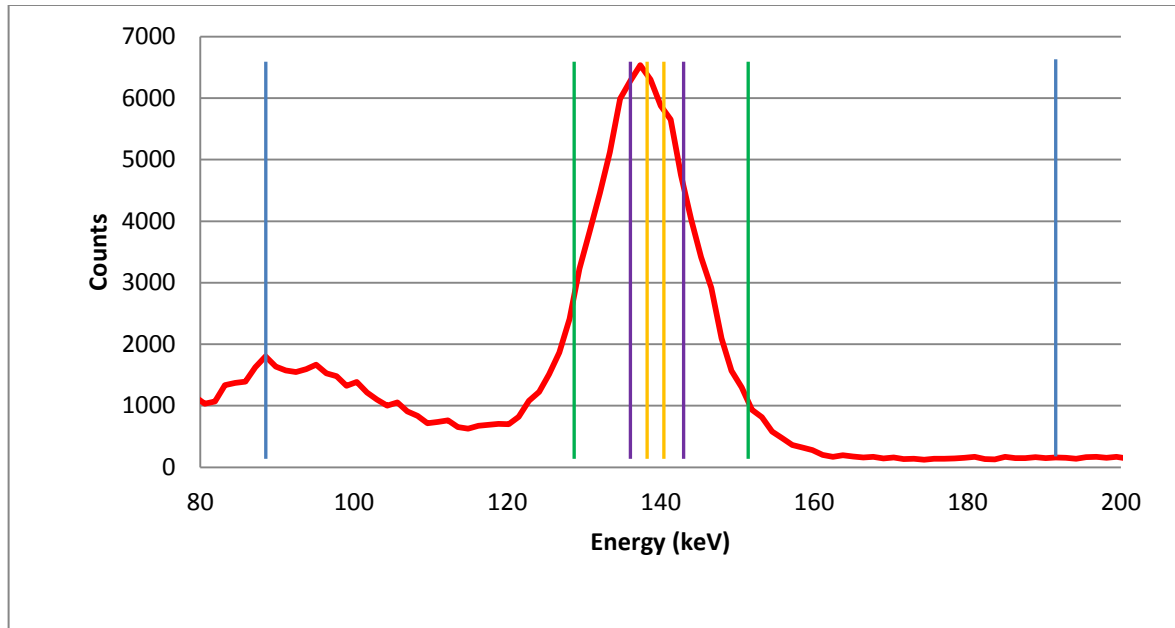


Fig. 3-3. Multiple energy window widths were used, varying the proportion of counts captured within the photopeak window relative to the total counts across the spectrum. Colored bars represent the different photopeak windows used: 2% (Orange), 6 % (Purple), 15% (Green), and 75% (Blue). The OW is not illustrated.

### 3.2.5 Method for Specific Aim I, Objective 5

#### 3.2.5.1 Method of data acquisition for Specific Aim I, Objective 5

To evaluate the effects of the incident energy spectrum on estimates of  $\tau$ , two Symbia detectors were evaluated using the Decay method with an OW under a series of different scatter conditions. In addition to the AIR and NEMA scatter conditions, the following three conditions were tested: The source placed in an acrylic scatter block ( $20 \times 20 \times 15$  cm), The source placed in an acrylic scatter block with 8.4 cm acrylic (7 sheets,  $1.2 \times 23 \times 23$  cm) placed between the block and the detector, and the source placed in an acrylic scatter block with a small lead shield (0.2 cm) positioned to attenuate radiation emitted in the direction of the detector but allow scattered radiation resulting in the relative reduction



of the photopeak. For each scatter condition, a spectrum was acquired on both detectors at or near the maximum observed count rate.

#### 3.2.5.2 Method of data analysis for Specific Aim I, Objective 4

$\tau$  was determined for the paralyzable portion of the CRP curves for all detectors using both the Rates and Counts methods. The energy spectra were used to calculate the effective energy for each scatter condition. The functional form of the dependence of  $\tau$  on effective energy was determined. The range in  $\tau$ , for the different effective energies used, was determined. Additionally, the change in effective energy that resulted in a 5% change in  $\tau$  was calculated.

### 3.3 Results for Specific Aim I

#### 3.3.1 *Results for Specific Aim I, Objective I*

The CRP curves for all three cameras tested were visually observed to agree with the PDM at low count rates. However, as input count rates increased, each system eventually reached a point where its behavior substantially deviated from the PDM (Fig. 3-4). The MCR that was observed for each of these systems occurred below the MCR predicted by the PDM. The lowest count rate data point measurements were performed at approximately 4 kcps. Based on estimates of  $\tau$  (Table 1), the losses due to dead time at this count rate were low (<0.5%).

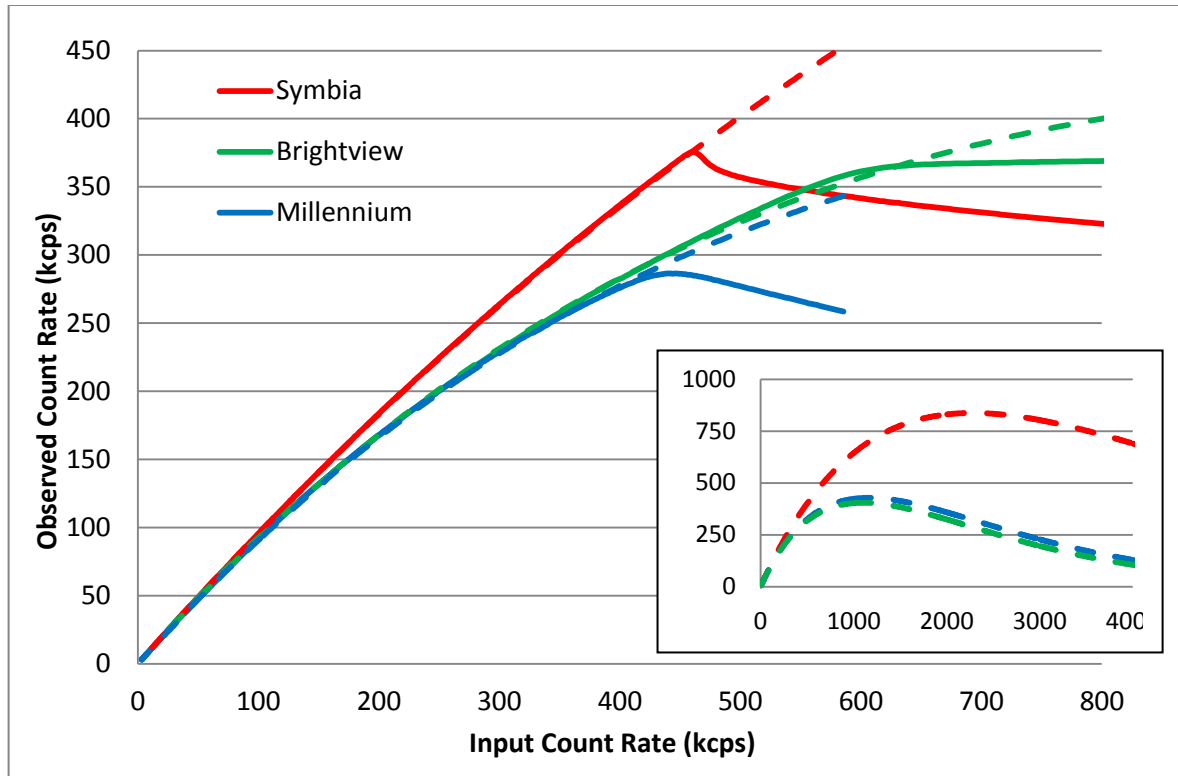


Fig. 3-4. The observed CRP curves for three modern gamma cameras (solid lines) are plotted along with the ideal CRP behavior predicted by the PDM (dashed lines). As higher input count rates are approached, all three gamma cameras have a distinct cutoff beyond which the system no longer follows the PDM. Relative to the Symbia, the Brightview and Millennium deviated more gradually from the PDM. The inset shows the behavior predicted by the PDM for these detectors at higher input count rates. The observed count rates increases with the input count rates, reaches a maximum, and then decreases. Unlike the observed behavior, the rollover at MCR for an ideal paralyzable detector occurs smoothly with no discontinuities and MCR may be calculated from Eqn. 2-8.

Table 3-3 shows the fitted estimates of  $\tau$  and MCR using both the Rates and Counts methods. Also shown are the measured MCR and the corresponding value of  $\tau$  for an ideal paralyzable detector. The measured background rate ( $b$ ) and initial input count rates ( $A_0$ ) estimated with the Rates method were found to be in good agreement with the values of  $b$  and  $A_0$  (fit parameters) using the Counts method. Values of  $A_0$  differed by 3% and the background rates differed by 1 kcps or less between the two methods. Also, the observed count rates at which the detector reached the 2% RMS residual criteria (see 3.2.1.2) are listed. These values differ by approximately 1% or less between the two methods.

Table 3-3. Dead time,  $\tau$  for the paralyzable portion of the CRP curve determined using both the Rates and Counts methods are tabulated with background count rate, initial input count rate, and the observed count rate where RMS residuals are less than 2% for both detectors of three different gamma cameras. Additionally, the MCR predicted from estimates of  $\tau$ , observed MCR, and  $\tau$  predicted from MCR using the PDM are tabulated to illustrate the differences between modern gamma camera performance and PDM predictions.

Camera	$\tau(\mu\text{s})$	$\tau$ Predicted from MCR ( $\mu\text{s}$ )	MCR (kcps)	MCR Predicted from $\tau$ (kcps)	Background Rate (kcps)	Initial Input Rate (kcps)	Observed Rate @ 2% RMS Residual (kcps)
<b>Rates</b>							
Symbia	0.439	0.978	376	838	0.626	869	354
Symbia	0.405	1.013	363	908	0.617	853	341
Brightview	0.859	0.927	397	428	1.419	6388	369
Brightview	0.857	0.951	387	429	1.352	5181	362
Millennium	0.909	1.286	286	405	0.232	620	277
Millennium	0.956	1.251	294	385	0.195	597	335
<b>Counts</b>							
Symbia	0.410	0.978	376	897	0.552	862	355
Symbia	0.376	1.013	363	979	0.541	846	342
Brightview	0.837	0.927	397	440	2.428	6197	370
Brightview	0.967	0.951	387	380	1.220	5187	365
Millennium	0.900	1.286	286	408	-0.023	618	280
Millennium	0.906	1.251	294	406	0.106	611	333

### 3.3.2 Results for Specific Aim I, Objective 2

Repeat measurements performed on the Symbia system using a Tc-99m source, OW, and the AIR spectral condition, resulted in a mean value of  $\tau = 0.441 \mu\text{s} \pm 0.00342 \mu\text{s}$  for detector 1 for the paralyzable portion of the CRP curve using the Rates method. Detector 2 had a mean value of  $\tau = 0.407 \mu\text{s} \pm 0.00256 \mu\text{s}$  using the Rates method. The Counts method resulted in mean values of  $\tau = 0.413 \mu\text{s} \pm 0.00324 \mu\text{s}$  and  $0.377 \mu\text{s} \pm 0.00121 \mu\text{s}$  for detectors 1 and 2 respectively. In all cases, the fractional error in the estimate of  $\tau$  was less than 1%.

### 3.3.3 Results for Specific Aim I, Objective 3

A high degree of correlation was observed between the Rates and Counts methods ( $r=0.9997$ ,  $p<0.001$ ). A plot of estimates of  $\tau$  using the Rates method vs. the Counts method is shown in Fig. 3-5. Fig. 3-6 shows a Bland-Altman plot with the difference between the two methods plot against its mean value. The mean difference in estimates of  $\tau$  between the rates and counts method for 42 different sets of measurements was calculated to be  $0.029 \pm 0.050 \mu\text{s}$ . The standard error in the mean difference was calculated to be  $0.008 \mu\text{s}$ . Given the number of data points used, the 95% confidence interval of the mean difference was between  $0.013$  and  $0.044 \mu\text{s}$ , indicating that the observed bias was statistically significant. This observation was confirmed by a two tailed t-test ( $p=0.0005$ ).

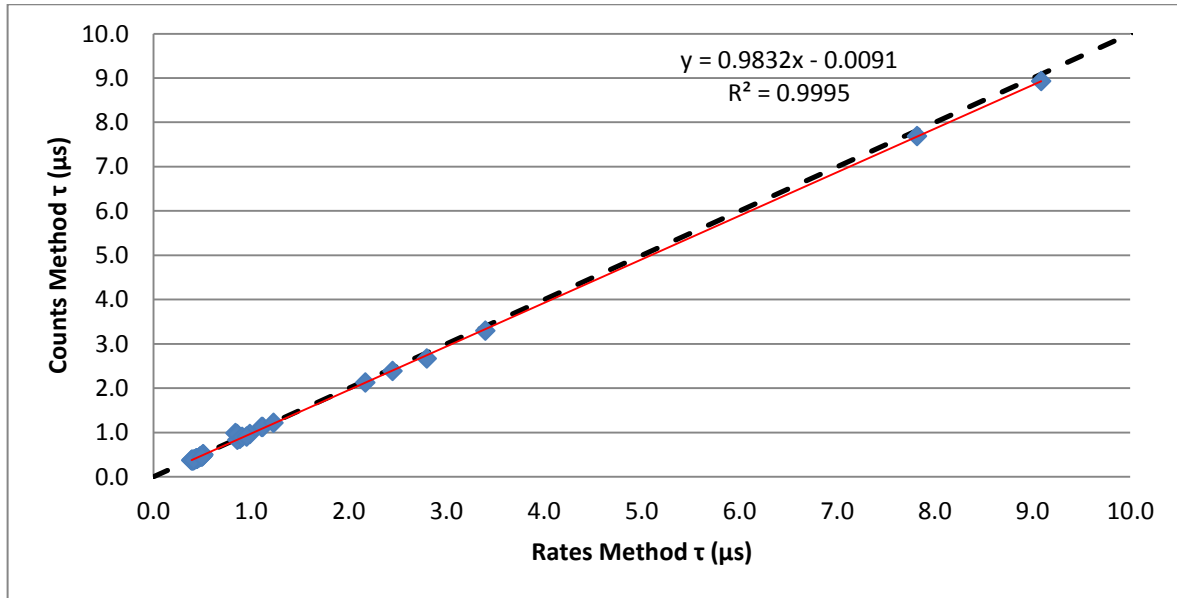


Fig. 3-5.  $\tau$  determined using the Rates method is plotted against  $\tau$  determined using the Counts method. The data plotted includes 42 Decay method data sets, utilizing various combinations of detector, spectral conditions, and energy window (Table 3-2). The red line represents the linear fit of the data from these methods. The dashed line represents perfect agreement between estimates of  $\tau$  using each method (line of identity).

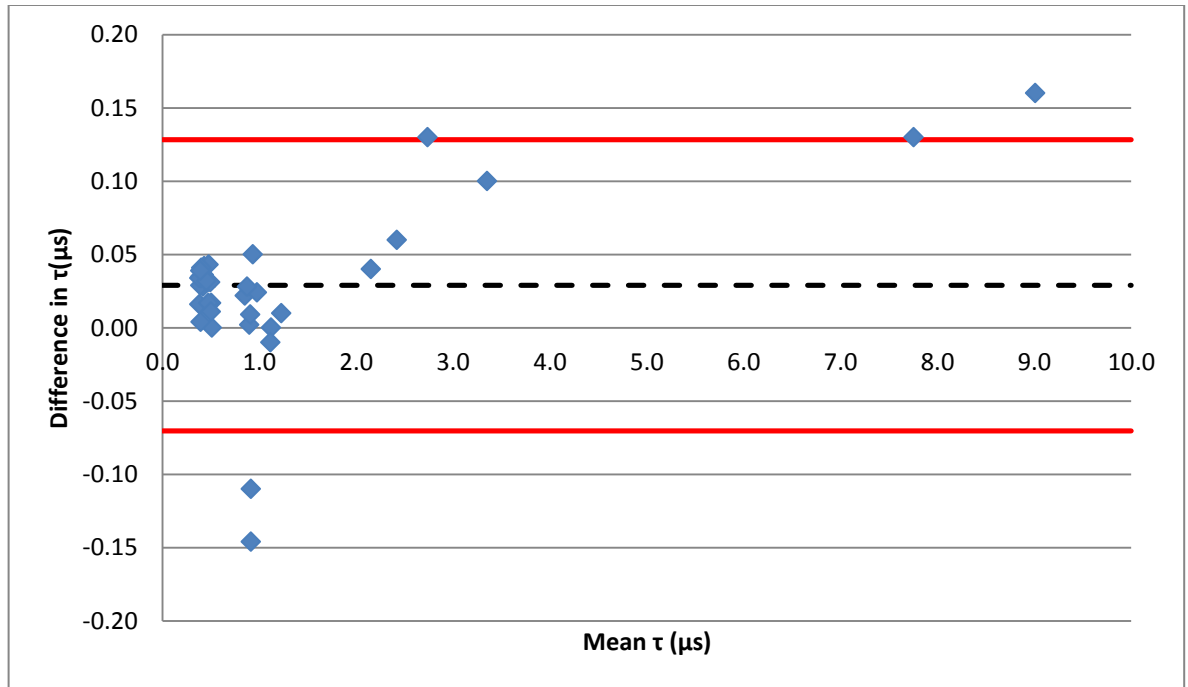


Fig. 3-6. Bland-Altman plot of agreement in  $\tau$  calculated using both the Rates and Counts method. The difference in  $\tau$  between the two estimates (ordinate) is plotted against their mean value (abscissa). The data plotted includes 42 Decay method data sets, utilizing various combinations of detector, spectral conditions, and energy window (Table 3-2). The dashed line represents the mean difference ( $\Delta\tau = 0.029 \mu\text{s}$ ) while the solid red lines represent  $\pm 2$  standard deviations ( $\sigma = 0.050 \mu\text{s}$ ).

### 3.3.4 Results for Specific Aim I, Objective 4

Energy window definition was observed to have a substantial effect on Decay method estimates of  $\tau$ . These estimates ranged from  $0.441 \mu\text{s}$  for an OW to  $7.82 \mu\text{s}$  for the 2% photopeak window for detector 1 and from  $0.407 \mu\text{s}$  for an OW to  $9.09 \mu\text{s}$  for the 2% photopeak window for detector 2. For both detectors this change in  $\tau$  is approximately 2000%.  $\tau$  was shown to be related to the ratio of photopeak window counts to total counts by a power law function as shown in Fig 3-7.  $\tau$  estimated for a 20% photopeak window deviated from a 15% photopeak window by 12.4% for detector 1 and 12.5% for detector 2.

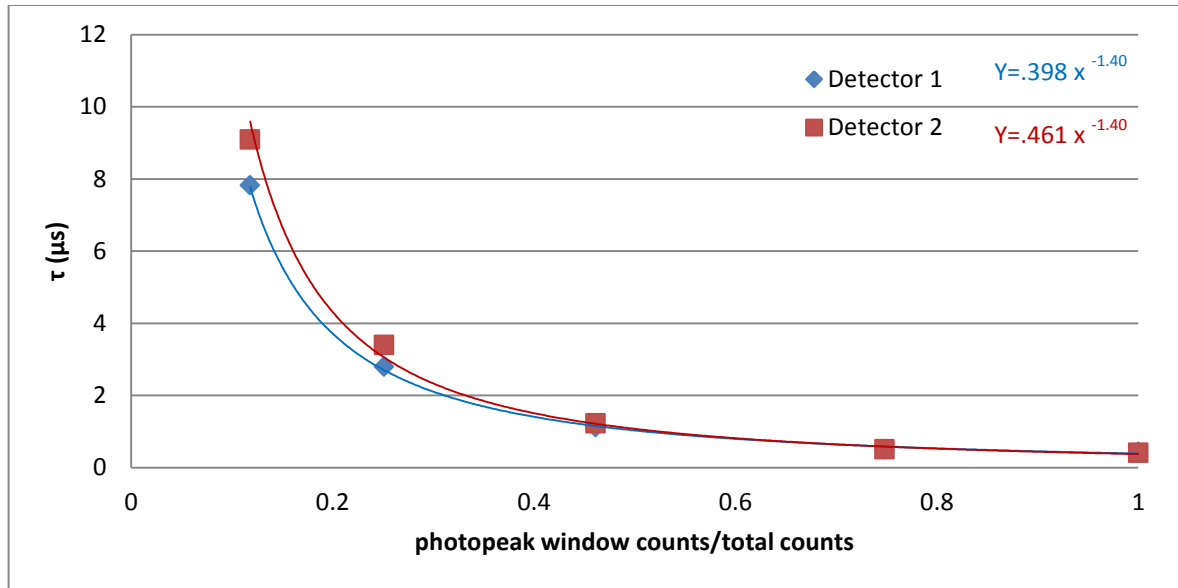


Fig. 3-7. The estimates of  $\tau$  plotted against the ratio of counts in the photopeak window to total counts in the spectrum (OW) for two Symbia 3/8 in. detectors using the Decay method. Data shown were acquired using a variety of energy windows intended to vary the proportion of counts captured within the window relative to the total counts across the entire spectrum.

### 3.3.5 Results for Specific Aim I, Objective 5

As the effective energy of the incident spectrum increases, the estimates of  $\tau$  were observed to decrease linearly in the range of 99.1 to 143 keV with values of  $\tau$  varying 17% for detector 1 and 19% for detector 2 (Fig. 3-8) using the Rates method. A 5% change in the value of  $\tau$  resulted from changes in effective energy of 11.8 keV for detector 1 and 10.6 keV for detector 2. Estimates of  $\tau$  varied by 2.53% and 2.24% for detectors 1 and 2 respectively between the AIR scatter condition and the NEMA scatter condition when using an OW.

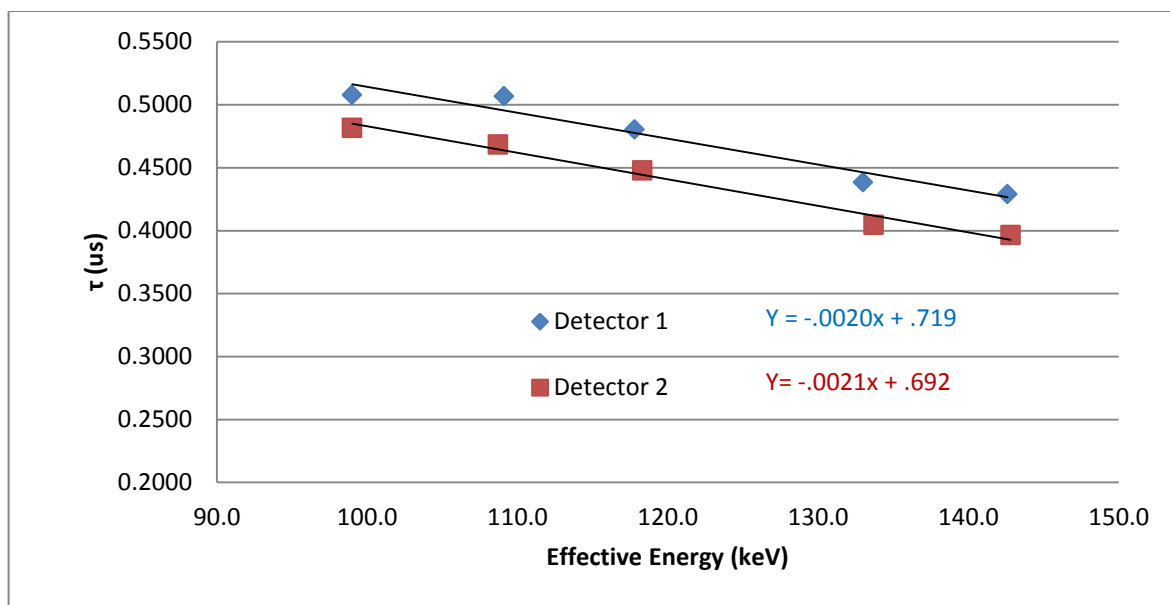


Fig. 3-8. The estimates of  $\tau$  plotted as a function of the effective energy of the incident spectrum using the Decay method for two Symbia 3/8 in. detectors. Data shown were acquired using an open energy window and 7 different spectral conditions were used to adjust the effective energy.

## 4. SPECIFIC AIM II

To investigate the effects of measurement conditions and acquisition parameters on the evaluation of count rate performance using the Dual Source method.

### 4.1 Objectives for Specific Aim II

To achieve Specific Aim II, five objectives were identified for investigation. Objectives 1 and 2 provide information necessary for the appropriate implementation of the Dual Source method while objectives 3-5 address the results of this method given different measurement conditions and acquisition parameters. All Dual Source measurements were performed on two uncollimated detectors of a Symbia gamma camera. The procedure began with a 30s background measurement. Next, measurements were made for five consecutive counting intervals, each of 5 seconds' duration, with the detectors exposed to source 1. These five measurements were repeated with the detectors exposed to both sources and then repeated again with the detectors exposed only to source 2. Another 30-second background measurement was performed. Five independent values for  $R_1$ ,  $R_2$ , and  $R_{12}$  were calculated by dividing the counts in each interval by its duration and subtracting the mean background count rate. The time between the first measurement of source 1 and the last measurement of source 2 was kept short ( $\Delta t < 1.5$  min) to minimize the effects of radioactive decay (during the measurement the source activity varied by less than 0.5%).

**4.1.1 Objective 1:** Identify the dependence of  $\tau$  on the ratio of activities of sources 1 and 2 to the total activity when estimated using the Dual Source method.



**4.1.2 Objective 2:** Identify the dependence of  $\tau$  on input count rate when estimated using the Dual Source method.

**4.1.3 Objective 3:** Evaluate the precision in  $\tau$ , estimated using the Dual Source method.

**4.1.4 Objective 4:** Identify the dependence of  $\tau$  on the energy window selected when estimated using the Dual Source method.

**4.1.5 Objective 5:** Identify the dependence of  $\tau$  on the incident energy spectrum when estimated using the Dual Source method with an open energy window.

## **4.2 Methods for Specific Aim II**

### **4.2.1 Method for Specific Aim II, Objective 1**

#### **4.2.1.1 Method of data acquisition for Specific Aim II, Objective 1**

To evaluate the dependence of  $\tau$ , estimated using the Dual Source method, on the degree of inequality of the source activities, the Dual Source method was performed on two Symbia detectors using an open energy window and two In-111 sources. In-111 was chosen because of its relatively long half-life compared to the duration of the experiment, which minimizes the effects of radioactive decay. The initial source activities were chosen such that source 1 contained approximately 90% of the total activity while source 2 contained approximately 10%. Dual Source measurements as described in section 4.1 were performed. Following these measurements, a fraction of the activity in source 1 was transferred to source 2, and the measurements were repeated. This process was repeated until source 1

contained approximately 14% of the total activity and source 2 contained 86%, resulting in 9 activity ratios. For each combination, the activity of sources 1 and 2 were measured in a dose calibrator and the ratio of the activity of source 1 to the total activity was determined.

#### 4.2.1.2 Method of data analysis for Specific Aim II, Objective 1

For each activity ratio, the mean value of  $\tau$  was calculated. The range of  $\tau$ , given the range of activity ratios used, was determined. The functional form of the dependence of  $\tau$  on the ratio of activity of source 1 to the total activity was determined. The ratios of the activity of source 1 to the total activity that resulted in a change in  $\tau$  of 1% and 5% from the value estimated when the activities of sources 1 and 2 were equal was determined.

### ***4.2.2 Methods for Specific Aim II, Objective 2***

#### 4.2.2.1 Method of data acquisition for Specific Aim II, Objective 2

To evaluate the dependence of  $\tau$  estimated using the Dual Source method on the count rate, the Dual Source method was performed on two Symbia detectors using two Tc-99m sources, an OW, and the AIR spectral condition. Activities were selected such that  $R_{12}$  was less than 5% of the maximum count rate. Dual Source measurements as described in section 4.1 were performed. Following data acquisition, the activity for both sources was increased and the measurements were repeated. This procedure was repeated until the combined activities of sources 1 and 2 provided an input count rate sufficient to exceed the MCR. The activities for source 1 and 2 were always within 2% of each other.

#### 4.2.2.2 Method of data analysis for Specific Aim II, Objective 2

The mean value of  $\tau$  was calculated at each level of total activity. A range of count rates where the estimates of  $\tau$  were relatively stable was identified. The functional form of the dependence of  $\tau$  on the total activity was determined for the stable range.

### **4.2.3 *Methods for Specific Aim II, Objective 3***

#### 4.2.3.1 Method of data acquisition for Specific Aim II, Objective 3

To evaluate the precision in the estimates of  $\tau$ , the Dual Source method was performed for two Symbia detectors using Tc-99m, an OW, the AIR spectral condition, and a total activity selected such that  $R_{12}$  was  $\sim 95\%$  of the MCR. The activities for source 1 and source 2 were within 2% of each other. Dual Source measurements as described in section 4.1 were performed, resulting in five separate measurements of  $R_1$ ,  $R_2$ , and  $R_{12}$ . Because each of these measurements was independent, 125 permutations of measured values of  $R_1$ ,  $R_2$ , and  $R_{12}$  are possible.

#### 4.2.3.2 Method of data analysis for Specific Aim II, Objective 3

$\tau$  was estimated for all 125 permutations of  $R_1$ ,  $R_2$  and  $R_{12}$  using Eqn. 2-10. The mean value, standard deviation, and fractional error of  $\tau$  were calculated.

### **4.2.4 *Methods for Specific Aim II, Objective 4***

#### 4.2.4.1 Method of data acquisition for Specific Aim II, Objective 4

To evaluate the dependence of  $\tau$ , estimated using the Dual Source method, on the energy window definition, the Dual Source method was performed for two Symbia detectors using four different photopeak window widths of 2%, 6%, 15%, and 75%, and an OW, a Tc-

99m point source, and the AIR scatter condition. The activities of sources 1 and 2 were maintained within 2% of each other and the total activity was selected such that the  $R_{12}$  was approximately 95% of MCR. The total activity varied by less than 5% between measurements made for each energy window. A spectrum was acquired with each detector with sufficient source activity such that the observed count rate was approximately 95% of the MCR.

#### 4.2.4.2 Method of data analysis for Specific Aim II, Objective 4

The mean value of  $\tau$  was calculated for each energy window. The energy spectra were used to compute the ratio of the counts in each photopeak window to the total counts (see Fig.3-3). The range of  $\tau$  for the energy windows used was determined. The functional form of the dependence of  $\tau$  on the ratio of photopeak window to total counts was determined. An estimate of  $\tau$ , for a 20% photopeak window, was computed from the functional form and the difference in  $\tau$  between the measured 15% window and the computed 20% window was calculated.

### 4.2.5 *Methods for Specific Aim II, Objective 5*

#### 4.2.5.1 Method of data acquisition for Specific Aim II, Objective 5

To evaluate the dependence of  $\tau$ , estimated using the Dual Source method, on the incident energy spectrum, the Dual Source method was performed for two Symbia detectors under seven different spectral conditions. Spectral conditions were modified through a combination of radionuclide (Tc-99m, In-111, or Tl-201) and the use of acrylic scattering material, lead shields, and copper filters. The measurements were performed twice with In-111, once using the AIR setup and once using the NEMA setup described in section 3.2.1.

The measurements were performed three times with Tc-99m, using both the AIR and NEMA setups and also by placing the source in an acrylic scatter block. The measurements were performed twice with Tl-201, once using the AIR setup and again by placing the source in the acrylic scatter block. Five trials were performed for each spectral condition using an OW for all acquisitions. Spectra were captured with the detectors exposed to both sources for each spectral condition. The activities for sources 1 and 2 were maintained within 2% of each other and the total activity was selected such that  $R_{12}$  was approximately 95% of the MCR. The total activity varied by less than 6% between scatter conditions.

#### 4.2.5.2 Method of data analysis for Specific Aim II, Objective 5

The mean value of  $\tau$  was calculated for each spectral condition. The energy spectra were used to calculate the effective energy for each scatter condition. The range of  $\tau$ , given the range in effective energies, was identified. The functional form of the dependence of  $\tau$  on effective energy was determined. The change in effective energy that resulted in a 5% change in  $\tau$  was calculated.

### 4.3 Results for Specific Aim II

#### 4.3.1 *Results for Specific Aim II, Objective 1*

The observed dependence of estimates of  $\tau$  on the ratio of the source activity to the total activity (Fig. 4-1) could be modeled as a quadratic function. Estimates of  $\tau$  varied 300% from 0.083  $\mu$ s with source 1 containing 90.4% of the total activity to 0.274  $\mu$ s with source 1 containing 50.4% of the total activity. Based on the fit, the estimates of  $\tau$  using the Dual Source method were within 5% of the maximum value when the ratio of source to total

activity was maintained between 39% and 61%, and  $\tau$  was within 1% of the maximum value when the ratio of source to total activity was maintained between 44% and 55%.

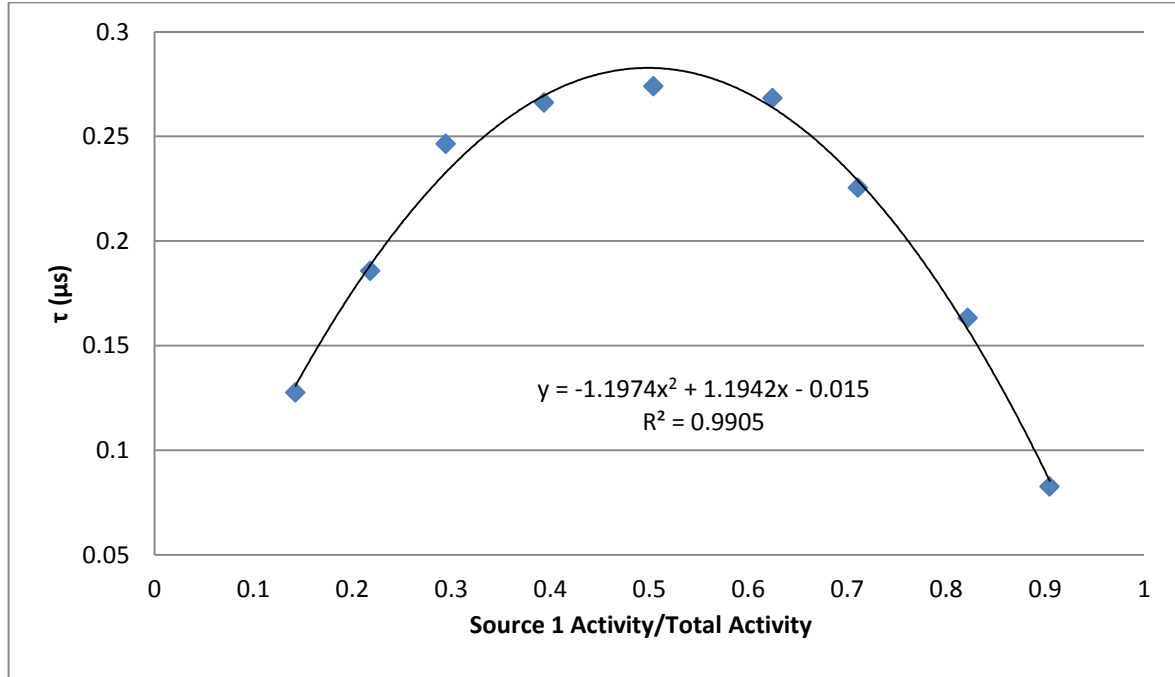


Fig. 4-1. The plot of  $\tau$ , estimated using the Dual Source method, using In-111 for a Symbia 3/8 in. detector plotted as a function of the ratio of source 1 activity to the total activity (source 1 + source 2). The data can be modeled as a quadratic function with a maximum value of  $\tau$  occurring at a ratio of single source activity to total activity of 0.50.

#### 4.3.2 Results for Specific Aim II, Objective 2

The Dual Source method estimates of  $\tau$  varied substantially with the total activity used (Fig. 4-2). Three distinct regions of behavior were observed. At lower activities where  $R_{12} < 35\%$  MCR, estimates of  $\tau$  decreased rapidly with lower activity and were subject to large fluctuations. For activities selected such  $R_{12} > 35\%$  MCR but still within the paralyzable portion of the CRP curve, estimates of  $\tau$  had a slowly varying linear dependence. At activities that resulted in count rates beyond the paralyzable portion of the CRP curve, values of  $\tau$  again increased rapidly. Within the relatively stable region where

$R_{12}$  was between 35% and 95% MCR, estimates of  $\tau$  ranged from 0.372  $\mu\text{s}$  to 0.430  $\mu\text{s}$  ( $\Delta\tau = 14.5\%$ ) for detector 1 and 0.360  $\mu\text{s}$  to 0.402 ( $\Delta\tau = 11.0\%$ )  $\mu\text{s}$  for detector 2.

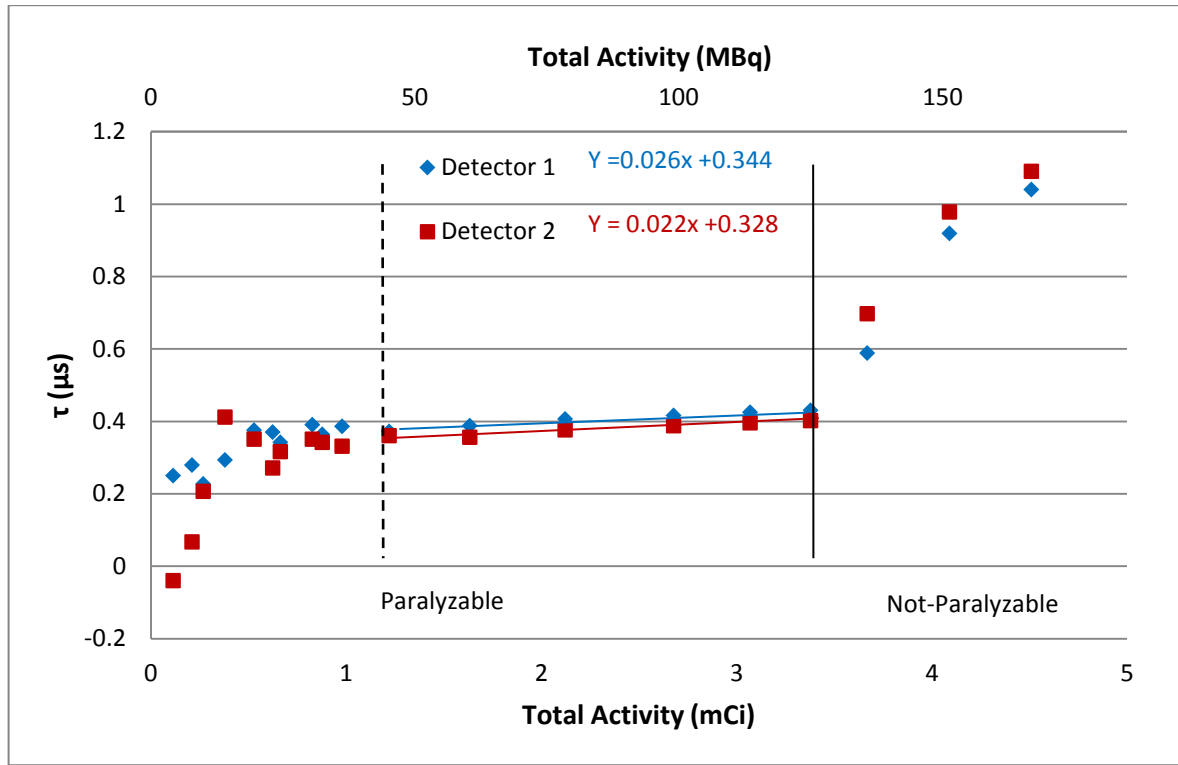


Fig.4-2. The plot of  $\tau$  estimated using the Dual Source method using Tc-99m for two Symbia 3/8 in. detectors plotted as a function of the total activity used. The stable region is indicated by the two vertical lines. The upper bound is indicated by the solid vertical line that corresponds to the activity at which  $\sim 95\%$  MCR is observed. The lower bound is indicated by the dashed line that corresponds to the activity at which  $\sim 35\%$  MCR is observed. When performing the Dual Source method, activities should be selected such that the total activity falls within the relatively stable region, preferably near the high count rate or activity region.

#### 4.3.3 Results for Specific Aim II, Objective 3

The mean value of  $\tau$  for the 125 permutations of  $R_1$ ,  $R_2$ , and  $R_{12}$  was  $0.430 \pm 0.002$   $\mu\text{s}$  and  $0.407 \pm 0.004$   $\mu\text{s}$  for detectors 1 and 2 respectively. For both detectors, the fractional error was less than 1%, similar to the precision of the Decay method.

#### 4.3.4 Results for Specific Aim II, Objective 4

The energy window definition was observed to have a substantial influence on the Dual Source method estimates of  $\tau$ . The estimates of  $\tau$  ranged from 0.434  $\mu\text{s}$  for an open energy window to 8.20  $\mu\text{s}$  for the 2% photopeak window for detector 1 and from 0.406  $\mu\text{s}$  for an open energy window to 11.17  $\mu\text{s}$  for the 2% photopeak window for detector 2 ( $\Delta\tau \sim 2000\%$ ).  $\tau$  was shown to be related to the ratio of photopeak window counts to total counts by a power law function (Fig.4-3).  $\tau$  estimated for a 20% photopeak window deviated from a 15% photopeak window by 12.6% for detector 1 and 12.9% for detector 2.

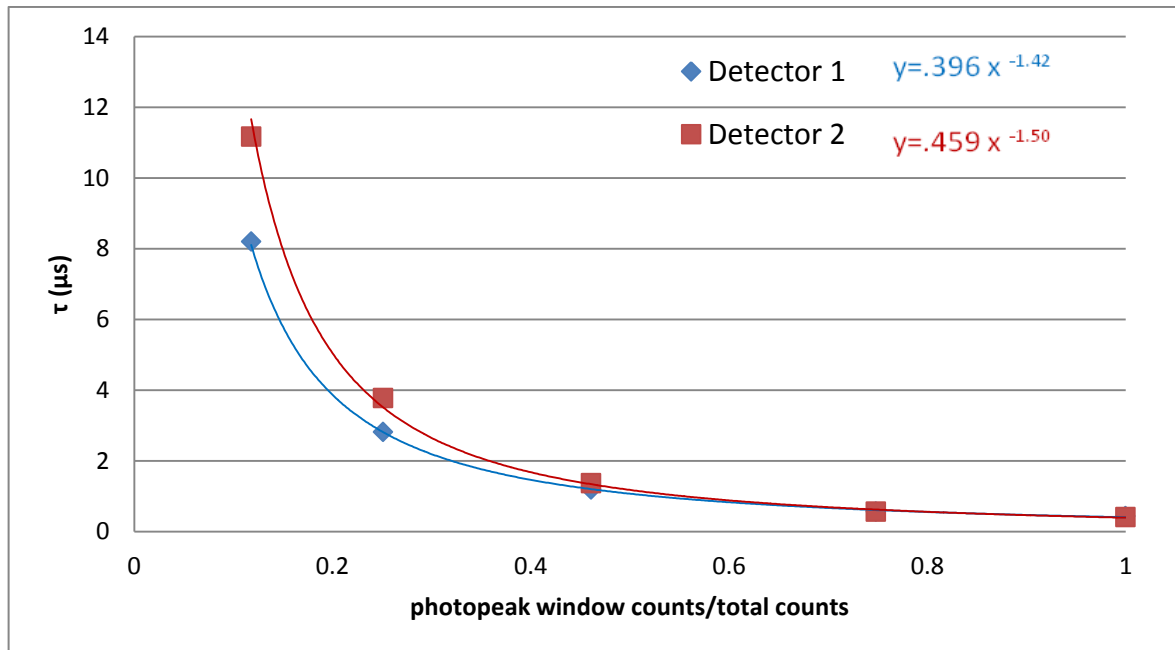


Fig. 4-3. The estimates of  $\tau$  plotted against the ratio of counts in the photopeak window to total counts in the spectrum (OW) for two Symbia 3/8 in. detectors using the Dual Source method. Data shown were acquired using a variety of energy windows intended to vary the proportion of counts captured within the window relative to the total counts across the entire spectrum.



#### 4.3.5 Results for Specific Aim II, Objective 5

As the effective energy of the incident spectrum increased, the estimates of  $\tau$  using the Dual Source method were observed to decrease linearly. In the range of 87.3 to 181.6 keV, values of  $\tau$  varied 43.4% for detector 1 and 42.5% for detector 2 (Fig. 4-4). A 5% change in the value of  $\tau$  resulted from changes in effective energy of 10.4 keV for detector 1 and 9.3 keV for detector 2.

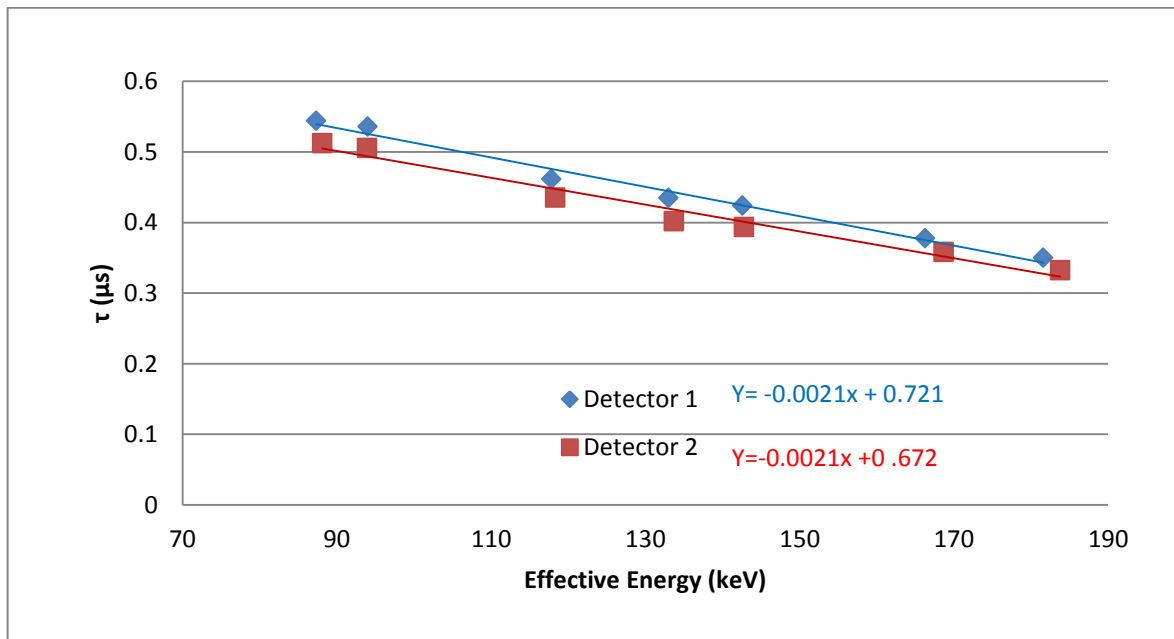


Fig. 4-4. The estimates of  $\tau$  plotted as a function of the effective energy of the incident spectrum using the Dual Source method for two Symbia 3/8 in. detectors. Data shown were acquired using an open energy window and 7 different spectral conditions used to adjust the effective energy.

## 5. Specific Aim III

To compare the results of the Decay method and the Dual Source method and to identify a technique for evaluating count rate performance that is appropriate for a clinical setting.

### 5.1 Objectives for Specific Aim III

To assess whether or not the Dual Source method may be used as a surrogate for the Decay method to estimate  $\tau$  for the paralyzable portion of the CRP curve, agreement between these methods was investigated. Additionally, for the methods to be considered interchangeable, the energy window and effective energy dependences that were observed in specific aims I and II should be independent of the method used to estimate  $\tau$ . To achieve this aim, the following three objectives were investigated:

**5.1.1 Objective 1:** Evaluate whether or not  $\tau$ , estimated using the Decay method and fitting rates, provides the same result as the Dual Source method, given fixed spectral conditions and energy windows.

**5.1.2 Objective 2:** Determine if the energy window dependence that was identified for estimates of  $\tau$  using the Decay method and fitting rates is the same as the energy window dependence that was identified for estimates of  $\tau$  using the Dual Source method.

**5.1.3 Objective 3:** Determine if the effective energy dependence that was identified for estimates of  $\tau$  using the Decay method and fitting rates is the same as the energy window dependence that was identified for estimates of  $\tau$  using the Dual Source method.

## 5.2 Methods for Specific Aim III

### 5.2.1 Method for Specific Aim III, Objective 1

#### 5.2.1.1 Method of data acquisition for Specific Aim III, Objective 1

$\tau$  was estimated for 25 combinations of gamma camera detector, energy windows and spectral conditions using both the Decay (Rates) and Dual Source methods (Table 5-1).

Table 5-1. The estimates of  $\tau$  for the paralyzable portion of the CRP curve using both the Decay (Rates) and Dual Source methods are tabulated with their difference and mean value for 25 combinations of camera, detector, incident spectrum and energy window.

Camera	Detector	Scatter Cond.	Energy Window	Rates $\tau$ ( $\mu$ s)	Dual Source $\tau$ ( $\mu$ s)	Difference ( $\mu$ s)	mean ( $\mu$ s)
Symbia S1	1	AIR	OW	0.389	0.392	-0.003	0.391
Symbia S1	1	NEMA	15% PW	0.896	0.964	-0.068	0.930
Symbia S1	2	AIR	OW	0.394	0.393	0.001	0.394
Symbia S1	2	NEMA	15% PW	1.110	0.946	0.164	1.028
Symbia S2	1	AIR	OW	0.439	0.434	0.005	0.436
Symbia S2	1	AIR	15% PW	1.120	1.189	-0.069	1.154
Symbia S2	1	NEMA	OW	0.430	0.424	0.006	0.427
Symbia S2	1	NEMA	15% PW	0.840	0.852	-0.012	0.846
Symbia S2	1	Scatter Block	OW	0.481	0.462	0.019	0.471
Symbia S2	1	Scatter Block	15% PW	2.170	2.240	-0.070	2.205
Symbia S2	1	AIR	2% PW	7.820	8.204	-0.384	8.012
Symbia S2	1	AIR	6% PW	2.800	2.815	-0.015	2.807
Symbia S2	1	AIR	75% PW	0.512	0.560	-0.048	0.536
Symbia S2	2	AIR	OW	0.405	0.406	-0.001	0.406
Symbia S2	2	AIR	15% PW	1.230	1.301	-0.071	1.266
Symbia S2	2	NEMA	OW	0.398	0.394	0.004	0.396
Symbia S2	2	NEMA	15% PW	0.987	1.000	-0.013	0.994
Symbia S2	2	Scatter Block	OW	0.448	0.436	0.012	0.442
Symbia S2	2	Scatter Block	15% PW	2.450	2.488	-0.038	2.469
Symbia S2	2	AIR	2% PW	9.090	11.172	-2.082	10.131
Symbia S2	2	AIR	6% PW	3.400	3.778	-0.378	3.589
Symbia S2	2	AIR	75% PW	0.506	0.564	-0.058	0.535
Symbia S4	1	AIR	OW	0.451	0.422	0.029	0.437
Symbia S4	2	AIR	OW	0.410	0.421	-0.011	0.416
Symbia T4	2	AIR	OW	0.887	0.862	0.025	0.875

#### 5.2.1.2 Method of data analysis for Specific Aim III, Objective 1

The mean difference, standard deviation of the differences, and the standard error of the mean difference were calculated. A paired t-test was performed to evaluate the significance of the mean difference. The degree of correlation between the two methods was evaluated by calculating the Pearson product moment correlation coefficient ( $r$ ). Additionally, a Bland-Altman analysis was performed to characterize the correlation between methods and to evaluate potential biases.

### 5.2.2 *Method for Specific Aim III, Objective 2*

#### 5.2.2.1 Method of data acquisition for Specific Aim III, Objective 2

Data used for this analysis were taken directly from Objective 4 of Specific Aims I and II. No additional data acquisition was required.

#### 5.2.2.2 Method of data analysis for Specific Aim III, Objective 2

To determine if there is a statistically significant difference in the dependence of  $\tau$  on the ratio of photopeak window counts to total counts, between the Decay (Rates) and Dual Source methods, values of  $\tau$  and the ratios were “linearized” by taking the natural logarithm of the data. These linearized values were then fit using linear least squares regression and the 95% confidence intervals were determined for the slopes and intercepts.

### 5.2.3 *Method for Specific Aim III, Objective 3*

#### 5.2.3.1 Method of data acquisition for Specific Aim III, Objective 3

Data used for this analysis were taken directly from Objective 5 of Specific Aims I and II. No additional data acquisition was required.

### 5.2.3.2 Method of data analysis for Specific Aim III, Objective 3

To determine if there is a statistically significant difference in the dependence of  $\tau$  on effective energy, between the Decay (Rates) and Dual Source methods, values of  $\tau$  and the effective energies for both methods were fit using linear least squares regression and the 95% confidence intervals were determined for the slopes and intercepts.

## 5.3 Results for Specific Aim III

### 5.3.1 Results for Specific Aim III, Objective 1

A high degree of correlation was observed between the Decay and Dual Source methods ( $r=0.9957$ ,  $p<0.001$ ) shown in Fig. 5-1. Fig. 5-2 shows a Bland-Altman plot with the difference between the Decay and Dual Source methods plotted against the mean value. The mean difference of the estimates of  $\tau$  between these methods for 25 different sets of measurements was calculated to be  $-0.131 \pm 0.420 \mu\text{s}$ . The standard error in the mean difference was calculated to be  $0.084 \mu\text{s}$ . Given the number of data points used, the 95% confidence interval of the mean difference was between  $-0.304$  and  $0.042 \mu\text{s}$ , indicating that the observed bias was not statistically significant. This observation was confirmed by a two tailed t-test ( $p=0.13$ ).

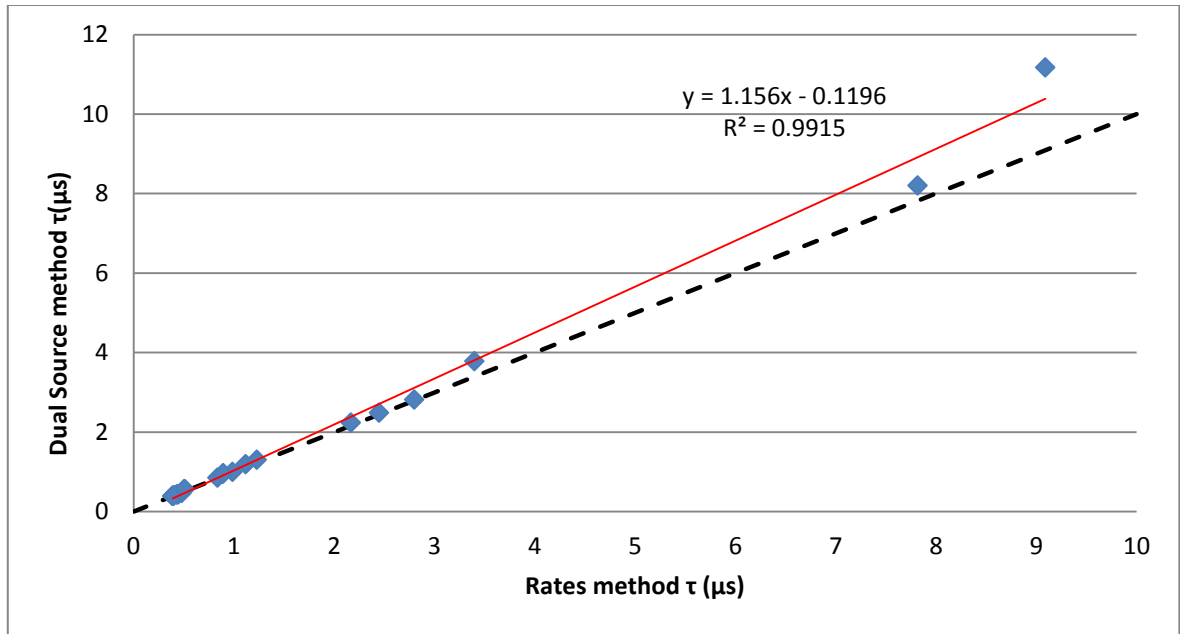


Fig. 5-1.  $\tau$  estimated using the Decay method (Rates) is plotted against  $\tau$  using the Dual Source method. The data plotted include 25 pairs of Decay and Dual Source method data sets. Each pair was estimated using the same detector, spectral conditions, and energy windows, while these parameters were varied between pairs (Table 5-1). The red line represents the linear fit for the paired data from these methods. The dashed line represents perfect agreement between estimates of  $\tau$  using each method (line of identity).

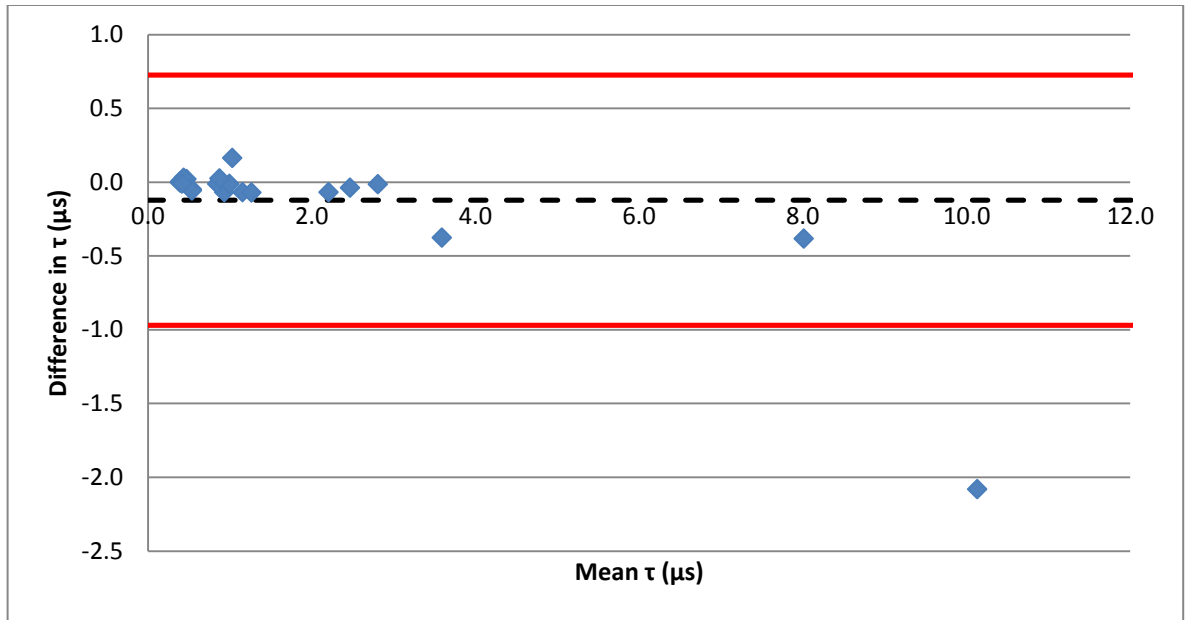


Fig. 5-2. Bland-Altman plot of agreement in  $\tau$  calculated using the Decay method (Rates) and Dual Source method. The difference in  $\tau$  between the two estimates (ordinate) is plotted against their mean value (abscissa). The data plotted include 25 pairs of Decay and Dual Source method estimates of  $\tau$ . Each pair was estimated using the same detector, spectral conditions, and energy windows, while these parameters were varied between pairs (Table 5-1). The dashed line represents the mean difference ( $\Delta\tau = -0.131 \mu\text{s}$ ) while the solid red lines represent  $\pm 2$  standard deviations ( $\sigma = 0.419 \mu\text{s}$ ).

### 5.3.2 Results for Specific Aim III, Objective 2

As seen in Figs. 5-3A and B, a linear relationship is observed when the natural logarithm of  $\tau$  is plotted against the natural logarithm of the ratio of the photopeak window to the total counts. Table 5-2 shows the slope, intercept, and their 95% confidence intervals for the Decay and Dual Source methods for both detectors. The linear fits for both the Decay (Rates) and Dual Source methods fell within the 95% confidence interval of each other for both detectors, indicating that there is no statistically significant difference between the relationships observed using these two methods.

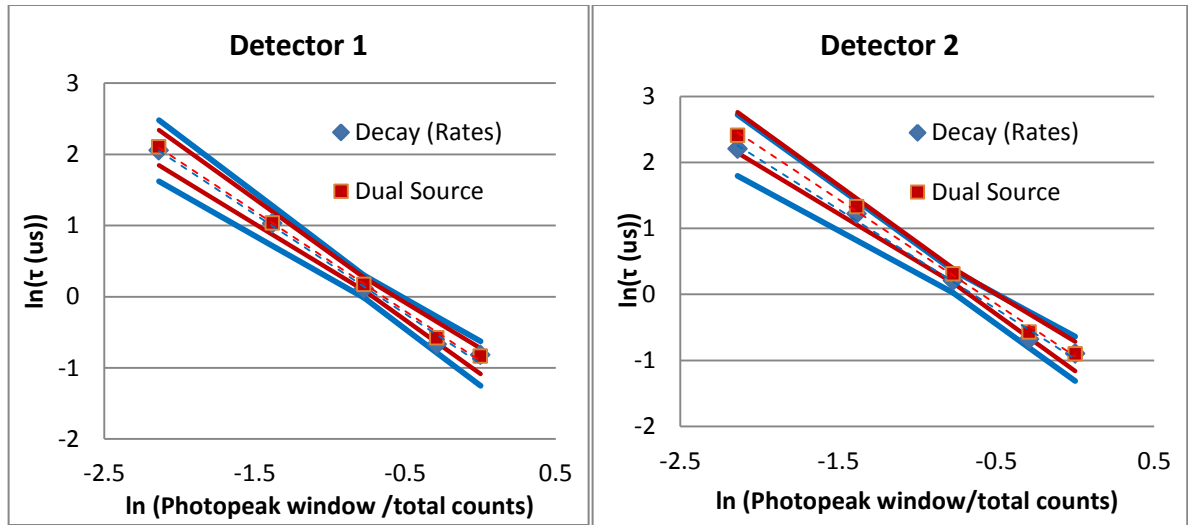


Fig. 5-3A(left) and Fig. 5-3B(right). The natural logarithm of  $\tau$  plotted against the natural logarithm of the ratio of counts in the photopeak window to the total counts for two Symbia 3/8 in. detectors. The dashed lines represent the least-squares fits to linear functions and the solid lines represent the 95% confidence intervals for these fits.

Table 5-2. Slope, intercept and their 95% confidence intervals (C.I.) for the linear dependence of the natural log of  $\tau$  on the natural log of the ratio of counts in the energy window to the total counts for the Decay (Rates) and Dual Source methods on both detectors.

	Slope		Intercept	
	mean	95% C.I.	mean	95% C.I.
<b>Detector 1 Decay (Rates)</b>	-1.400	-1.601 to -1.199	0.143	-0.014 to 0.300
<b>Detector 1 Dual Source</b>	-1.404	-1.519 to -1.288	0.180	0.089 to 0.270
<b>Detector 2 Decay (Rates)</b>	-1.516	-1.732 to -1.299	0.196	0.026 to 0.365
<b>Detector 2 Dual Source</b>	-1.590	-1.733 to -1.446	0.290	0.178 to 0.402

### 5.3.3 Results for Specific Aim III, Objective 3

Figs. 5-4A and 5-4B show the linear fits of  $\tau$  versus effective energy for each detector using both methods and the corresponding 95% confidence intervals for those fits. Table 5-3 lists the slope, intercept, and their 95% confidence intervals for the Decay and Dual Source methods for both detectors. The linear fits for both the Decay and Dual Source



methods fall within the 95% confidence intervals of each other for both detectors, indicating that there is no statistically significant difference between the relationships observed using these two methods.

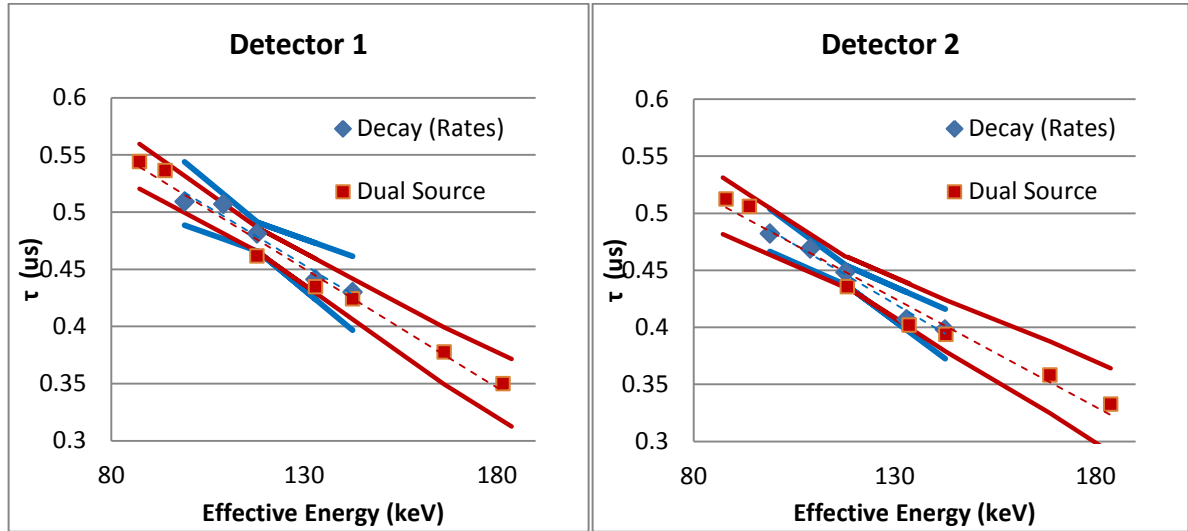


Fig. 5-4A(left) and Fig.5-4B(right). The estimates of  $\tau$  plotted against the effective energy of the incident spectrum using the Decay and Dual Source methods for two Symbia 3/8 in. detectors. The dashed lines represent the least-squares fit to linear functions and the solid lines represent the 95% confidence intervals for these fits.

Table 5-3. Slope, intercept, and their 95% confidence intervals (C.I.) for the linear fits of the dependence of  $\tau$  on effective energy for the Decay (Rates) and Dual Source methods on both detectors.

	Slope		Intercept	
	mean	95% C.I.	mean	95% C.I.
<b>Detector 1 Decay (Rates)</b>	-0.239	-0.325 to -0.153	0.717	0.629 to 0.805
<b>Detector 1 Dual Source</b>	-0.256	-0.305 to -0.207	0.731	0.678 to 0.783
<b>Detector 2 Decay (Rates)</b>	-0.244	-0.302 to -0.187	0.631	0.631 to 0.749
<b>Detector 2 Dual Source</b>	-0.244	-0.268 to -0.181	0.622	0.622 to 0.723

## **6. SPECIFIC AIM IV**

To investigate the effects of high count rates on gamma camera quality assurance metrics.

### **6.1 Objectives for Specific Aim IV**

To investigate the effects of count rate on the performance of modern gamma cameras, three performance metrics (uniformity, intrinsic spatial resolution, and energy resolution) were selected for evaluation. These metrics were chosen because they can be evaluated intrinsically, allowing for relatively high count rates to be achieved without extremely high activity sources and based on their likelihood to be effected by high count rates. The fourth objective was chosen to provide a basic assessment of the image distorting effects of high count rates.

**6.1.1 Objective 1:** Evaluate the effects of count rate losses on image uniformity.

**6.1.2 Objective 2:** Evaluate the effects of count rate losses on spatial resolution.

**6.1.3 Objective 3:** Evaluate the effects of count rate losses on energy resolution and photopeak energy.

**6.1.4 Objective 4:** Evaluate image distortion caused by high count rates.

## **6.2 Methods for Specific Aim IV**

### **6.2.1 Method for Specific Aim IV, Objective 1**

#### **6.2.1.1 Method of data acquisition for Specific Aim IV, Objective 1**

To evaluate the effects of count rate losses on image uniformity, a 10 million count image was acquired on an uncollimated Symbia detector using a Tc-99m source, the AIR scatter condition, a 15% photopeak window, and a matrix size of 1024\*1024. Source activity was selected such that the observed count rate was less than 10% of the MCR. Once the image had been acquired, the activity was increased and the acquisition was repeated. This procedure was iterated until the activity was approximately 400% of what was required to obtain the MCR.

#### **6.2.1.2 Method of data analysis for Specific Aim IV, Objective 1**

Following data acquisition, useful field of view integral uniformity (UFOV INT), useful field of view differential uniformity (UFOV DIFF), central field of view integral uniformity (CFOV INT), and central field of view differential uniformity (CFOV DIFF) were calculated for each image in accordance with NU1-2007<sup>2</sup>. The range in each measure of uniformity was determined for the paralyzable portion of the CRP curve. The dependence of each measure of uniformity on activity (proportional to input count rate) was identified via linear least-squares regression for both the entire range and for the paralyzable portion of the CRP curve. An *F*-test was performed to determine if the slopes of the regression lines were significantly non-zero.

## **6.2.2 Method for Specific Aim IV, Objective 2**

### **6.2.2.1 Method of data acquisition for Specific Aim IV, Objective 2**

To investigate the effects of count rate losses on spatial resolution a lead straight edge was placed on an uncollimated Symbia detector. The edge response function was used to evaluate spatial resolution. A 10 million count image was acquired using a Tc-99m source, the AIR scatter condition, a 15% photopeak window, and a matrix size of 1024\*1024. The source activity was selected such that the observed count rate was less than 10% of the MCR. Once the image had been acquired, the activity was increased and the acquisition was repeated. This procedure was iterated, until the activity was well beyond what was required to obtain the MCR.

### **6.2.2.2 Method of data analysis for Specific Aim IV, Objective 2**

Because the lead straight edge did not extend across the entire horizontal distance of the detector, a truncated image (Figs. 6-1A and B) was used such that the region of low intensity pixels resulting from the edge was present in each vertical column. The mean pixel value was determined for each horizontal row of pixels to generate the average signal profile across the Pb strip as a function of position (1 Pixel = 0.599 mm). This profile represents the edge spread function (Fig. 6-2A). The first derivative of this function was taken to obtain the line spread functions to evaluate spatial resolution of the system at the edge interface, resulting in a Gaussian positioned at each edge of the low intensity region (Fig. 6-2B). The Gaussian from the upper edge was fit numerically and the full width at half maximum (FWHM) was calculated. The FWHM was plotted against activity and fit using linear least-squares regression and the range in FWHM was determined for the paralyzable

portion of the CRP curve and for the entire data set. An  $F$ -test was performed to determine if the slope of the regression line was significantly non-zero.

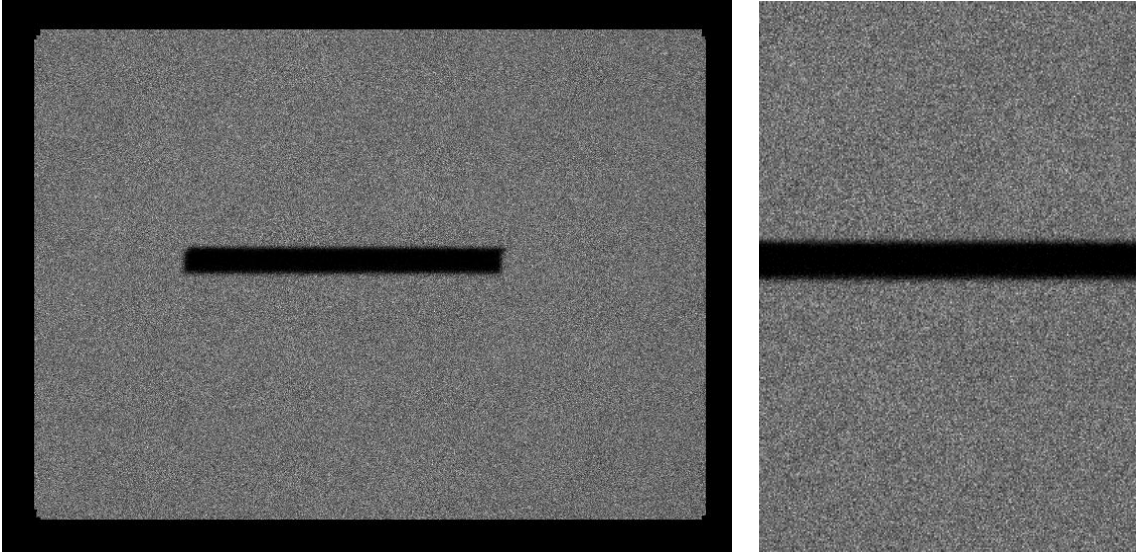


Fig. 6-1A (left) and B (right). The image generated with the lead straight edge placed on the uncollimated detector (6.1A) is shown with the associated truncated image used to make measurements (6.1B).

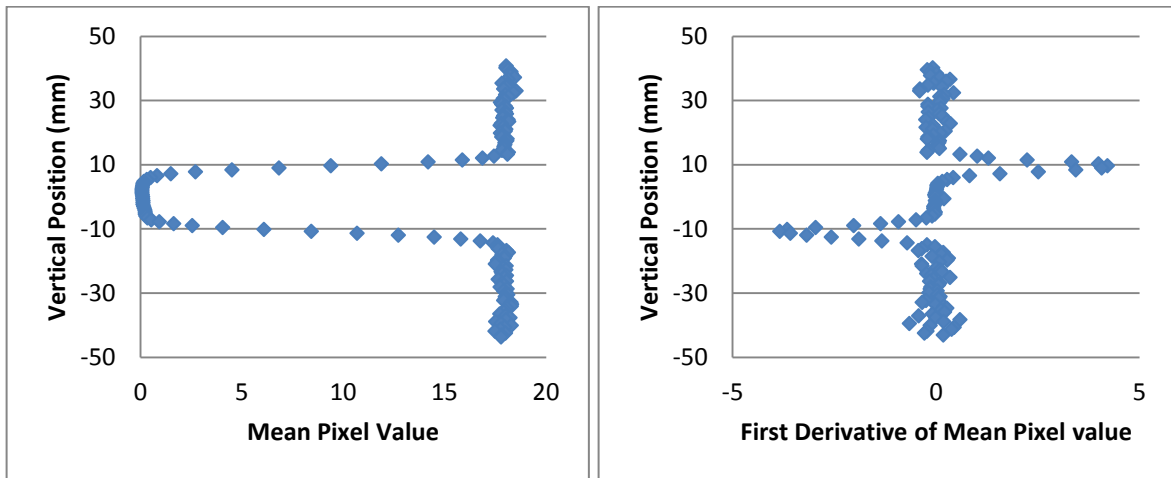


Fig. 6-2 A (left) and B (right). Plot of the edge response function (Fig. 6.2A) measured from Fig. 6.1B and its derivative (Fig. 6.2B).

### **6.2.3 Method for Specific Aim IV, Objective 3**

#### **6.2.3.1 Method of data acquisition for Specific Aim IV, Objective 3**

To evaluate the effects of count rate losses on energy resolution and photopeak energy, spectra were acquired on an uncollimated Symbia detector using a Tc-99m source and the NEMA scatter condition over a range of activities.

#### **6.2.3.2 Method of data analysis for Specific Aim IV, Objective 3**

Following acquisition, the Tc-99m photopeak region in each spectrum was fit with a Gaussian plus a linear function. The FWHM was calculated from this fit and the photopeak energy was identified. The range in FWHM and photopeak energy for the paralyzable portion of the CRP curve was determined. The dependence of the energy resolution and the photopeak energy on activity was identified using linear least squares regression and an *F*-test was performed to determine if the slope of the regression lines were significantly non-zero.

### **6.2.4 Method for Specific Aim IV, Objective 4**

#### **6.2.4.1 Method of data acquisition for Specific Aim IV, Objective 4**

To evaluate the image distortion that results from high count rates, an uncollimated Symbia detector was exposed to two Tc-99m point sources placed in lead containers with an opening facing the detector and positioned approximately 10 cm apart (Figs. 6.3A and B). The containers were used so that the radiation incident on the detector would be highly collimated. The source activity was selected such that the input count rate was less than 10% of MCR. A 10 million count image was acquired using the 15% photopeak window. After acquisition, the activity of both sources was increased and imaging was repeated. Source

activities were maintained within 2% of each other at all times. This procedure was repeated until the activity was approximately 800% of what was required to obtain the MCR.

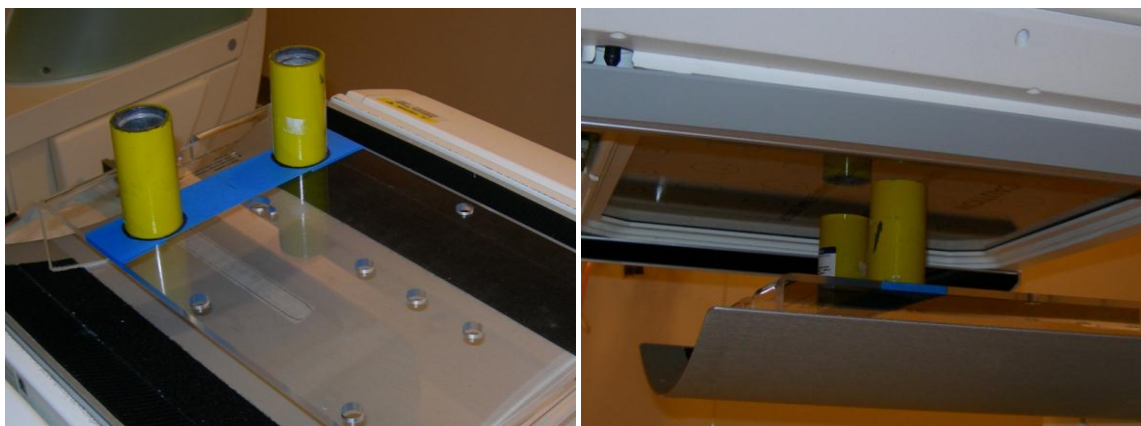


Fig. 6-3A (left) and B (right). Photographs of the experimental set up for evaluating image distortion are shown here. Sources are positioned at a fixed distance for the duration of the experiment.

#### 6.2.4.2 Method of data analysis for Specific Aim IV, Objective 4

Regions of Interest (ROIs) were drawn around each of the two sources in the acquired images and the center of mass of the counts from each source was determined (Fig. 6-4). Additionally, a third ROI was drawn directly between the activity distributions of the two sources and the maximum pixel value in it was determined. The ratio of the maximum pixel value measured in the central ROI to the maximum pixel value from the entire image was calculated. The horizontal position of source 1 was plotted against the total activity and fit using linear least-squares regression. An  $F$ -test was performed to determine if the slope of the regression line was significantly non-zero.

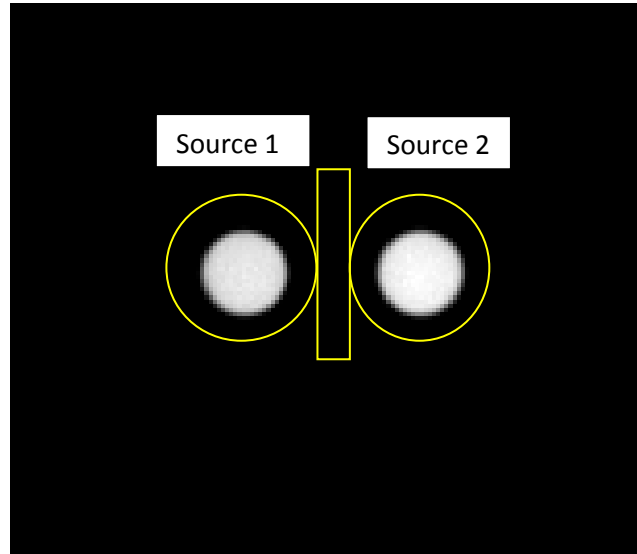


Fig. 6-4 An image of the two sources used to evaluate distortion is shown to illustrate placement of ROIs.

### 6.3 Results for Specific Aim IV

#### 6.3.1 Results for Specific Aim IV, Objective 1

All measures of uniformity degraded with activity and hence input count rate over the entire range of activities. However, the slope of the regression lines for the paralyzable portion of the CRP curve was found to be significantly non-zero only for the UFOV INT measurement (Fig. 6-5A-D). Also, measurements of uniformity become substantially noisier beyond the MCR as illustrated in Figs. 6-6A-D. The minimum uniformity value, maximum value below the MCR, maximum values for the entire data set, slope of the regression lines and  $F$  statistics and the corresponding  $P$  values are listed in Table 6.1.



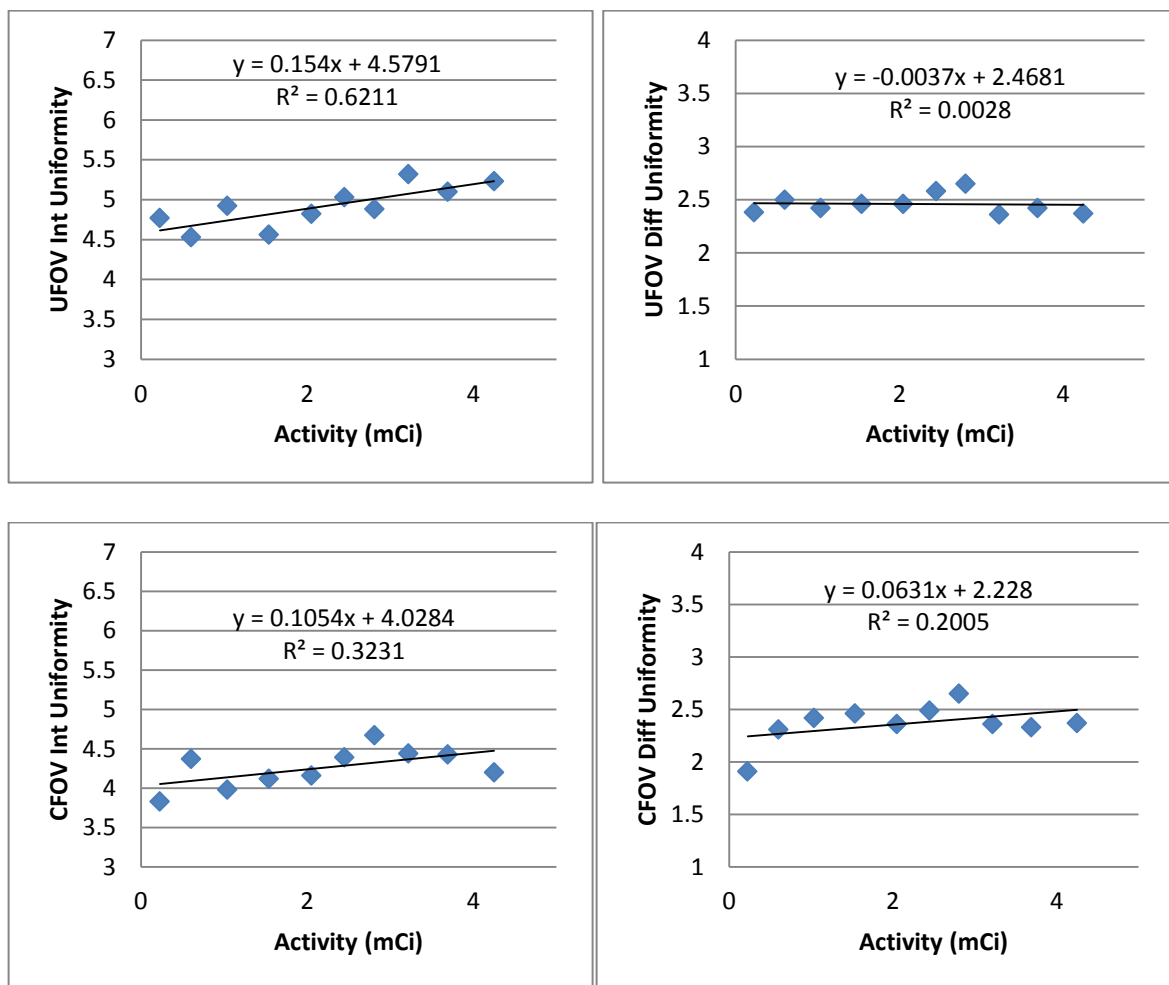


Fig. 6-5 A (upper left), B (upper right), C (lower left), and D (lower right). Integral and differential uniformity calculated for the useful (A and B) and central (C and D) fields of view as defined in NU1-2007 are plotted against activity for the paralyzable portion of the CRP curve.

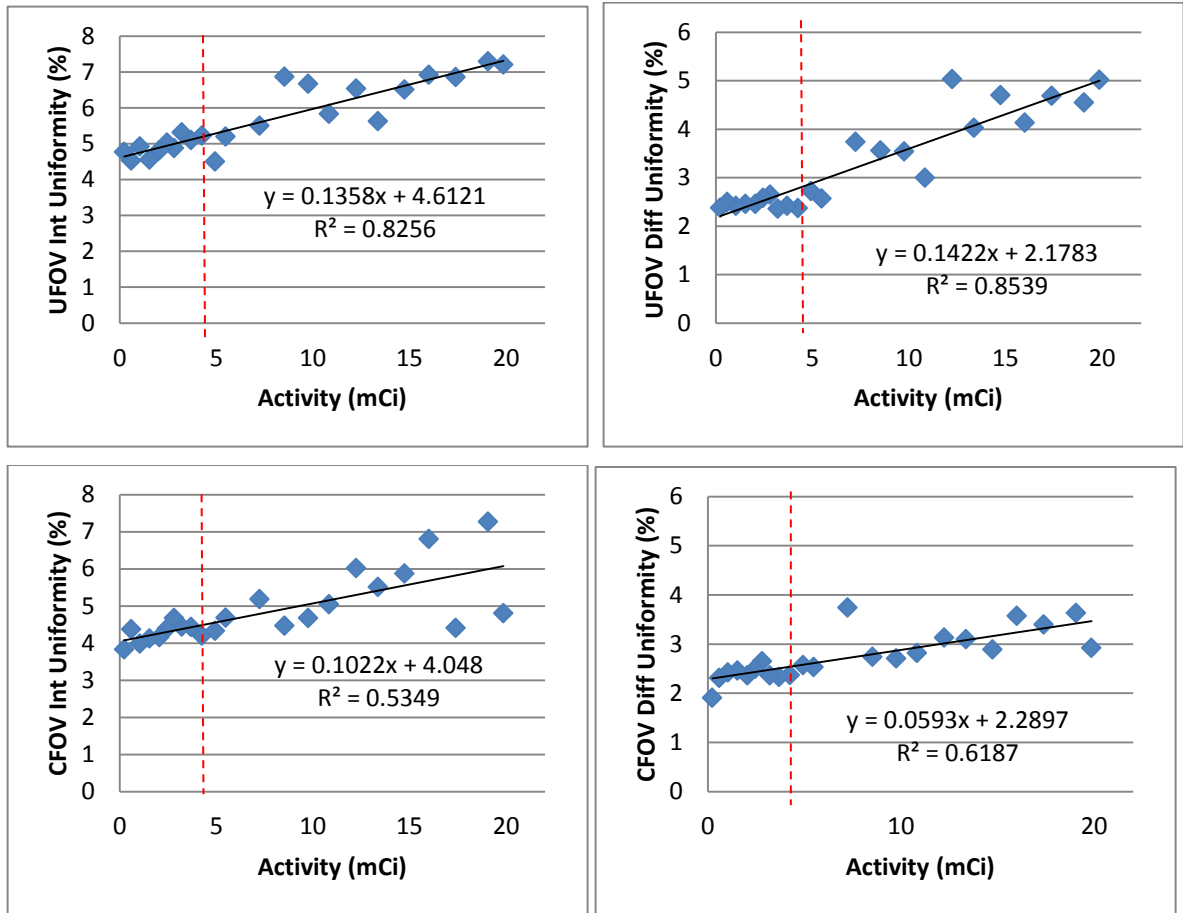


Fig. 6-6 A (upper left), B (upper right), C (lower left), and D (lower right). Integral and differential uniformity calculated for the useful and central fields of view as defined in NU1-2007 are plotted against activity for the entire tested range. The dashed lines indicate the activity at which MCR occurs.

Table 6-1. The minimum and maximum uniformity values, slope of the regression lines, and  $F$  statistics and corresponding  $P$  value are tabulated for each data set for both the entire range and the paralyzable portion of the CRP curve.

<b><u>Full Range</u></b>	<b><u>Minimum (%)</u></b>	<b><u>Maximum (%)</u></b>	<b><u>Slope</u></b>	<b><u>F</u></b>	<b><u>P</u></b>
<b>UFOV INT</b>	4.53	7.3	0.136	99.4	<0.001
<b>UFOV DIFF</b>	2.36	5.03	0.142	122.7	<0.001
<b>CFOV INT</b>	3.83	7.27	0.102	24.2	<0.001
<b>CFOV DIFF</b>	1.91	3.74	0.059	34.1	<0.001
<b><u>Paralyzable Range</u></b>					
<b>UFOV INT</b>	4.53	5.32	0.154	13.11	0.007
<b>UFOV DIFF</b>	2.36	2.65	-0.004	0.022	0.885
<b>CFOV INT</b>	3.83	4.67	0.105	3.82	0.086
<b>CFOV DIFF</b>	1.91	2.65	0.063	2.01	0.194

### **6.3.2 Results for Specific Aim IV, Objective 2**

The intrinsic spatial resolution FWHM was observed to degrade linearly with activity and hence input count rate over the entire range of activities tested as shown in Fig. 6.7. The FWHM ranged from 3.70 to 4.23 mm for the paralyzable portion of the CRP curve and up to 5.80 mm for the entire data set. The slope of the regression line was determined to be significantly non-zero ( $F = 658.5$ ,  $P < 0.001$ ). No change in behavior was observed between paralyzable and non-paralyzable portions of the CRP curve.

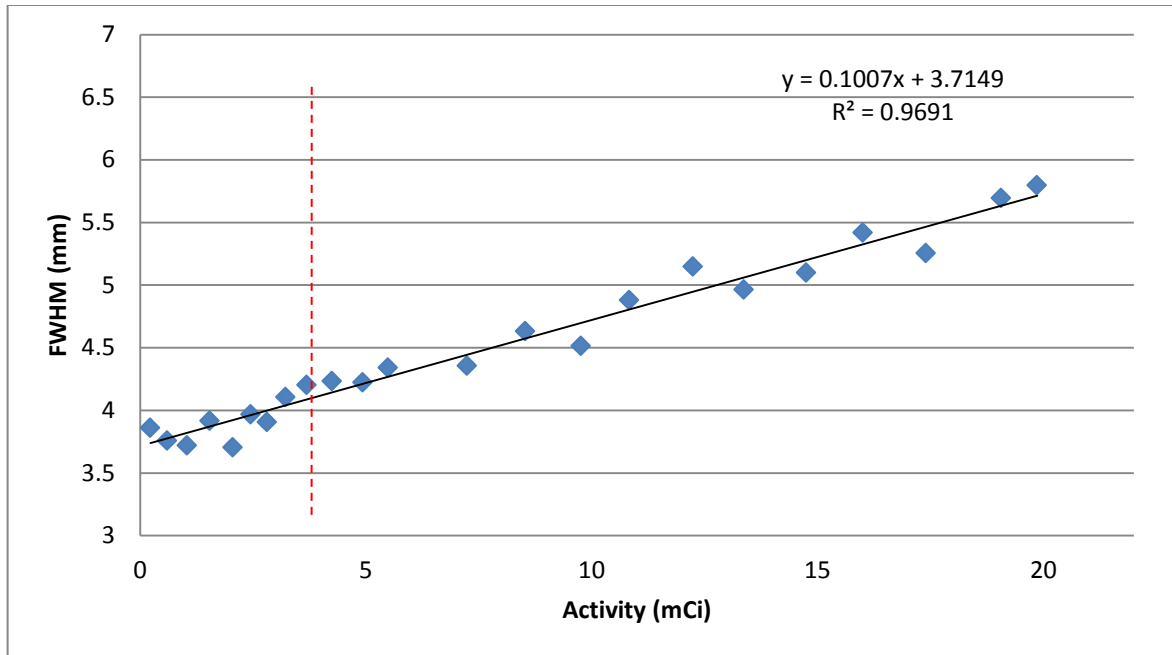


Fig. 6-7. FWHM of the line spread function obtained from the Gaussian fit of the first derivative of edge spread function of a lead straight edge is plotted against activity. The dashed line indicates the activity at which the MCR occurred.

### 6.3.3 Results for Specific Aim IV, Objective 3

The energy resolution FWHM degraded linearly with activity and hence the input count rate over the entire range of activities tested as shown in Fig. 6-8. The FWHM of the Tc-99m photopeak ranged from 11.02% to 13.57% for the paralyzable portion of the CRP curve. The photopeak energy increased linearly with activity and hence count rate over the entire range of activities tested as shown in Fig. 6-9. Photopeak energy ranged from 138.1 keV to 139.7 keV for the paralyzable portion of the CRP curve. The slopes of the regression lines were determined to be significantly non-zero for both energy resolution FWHM ( $F = 7143$ ,  $P < 0.001$ ) and photopeak energy ( $F = 901.6$ ,  $P < 0.001$ ). No change in behavior was observed between the paralyzable and non-paralyzable portions of the CRP curve for either plot.

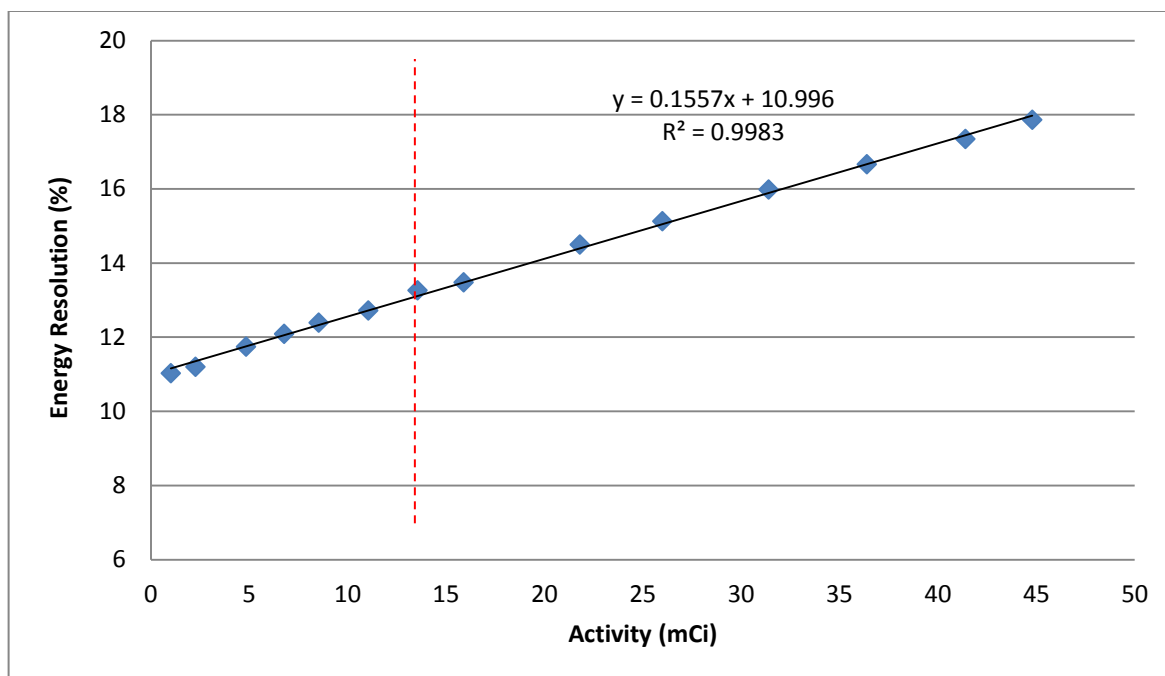


Fig. 6-8. FWHM of a Gaussian plus a linear fit to the Tc-99m photopeak is plotted against activity. The dashed line indicates the activity at which MCR occurred.

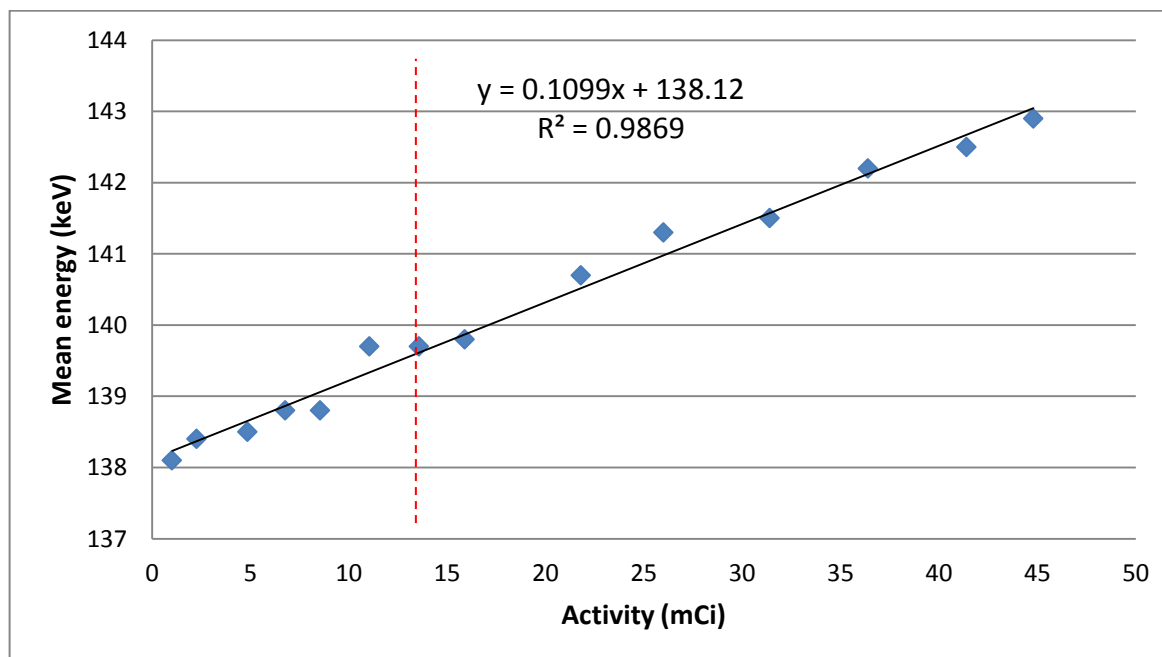


Fig. 6-9. Photopeak energy of the Tc-99m photopeak plotted against activity. The dashed line indicates the activity at which the MCR occurred.

#### **6.3.4 Results for Specific Aim IV, Objective 4**

The horizontal position of the center of mass of the counts of source 1 was observed to shift linearly with activity and hence input count rate over the entire range of activities tested as shown in Fig. 6-10. This position ranged from 253.6 mm to 258.6 mm ( $\Delta=2\%$ ) for the paralyzable portion of the CRP curve and up to 267.1 mm ( $\Delta=5\%$ ) for the entire data set. The slope of the regression line was determined to be significantly non-zero ( $F = 205.7$ ,  $P < 0.001$ ). No change in behavior was observed between the paralyzable and non-paralyzable portions of the CRP curve. Also, the ratio of maximum pixel value in the central ROI to the maximum in the entire image was shown to increase with activity and hence input count rate as shown in Fig. 6-11. This ratio ranged from 0.1% to 0.6% for the paralyzable portion of the CRP curve and up to 5.3% for the entire data set. Fig. 6-12 illustrates both the distorting and mispositioning effects of high count rates.

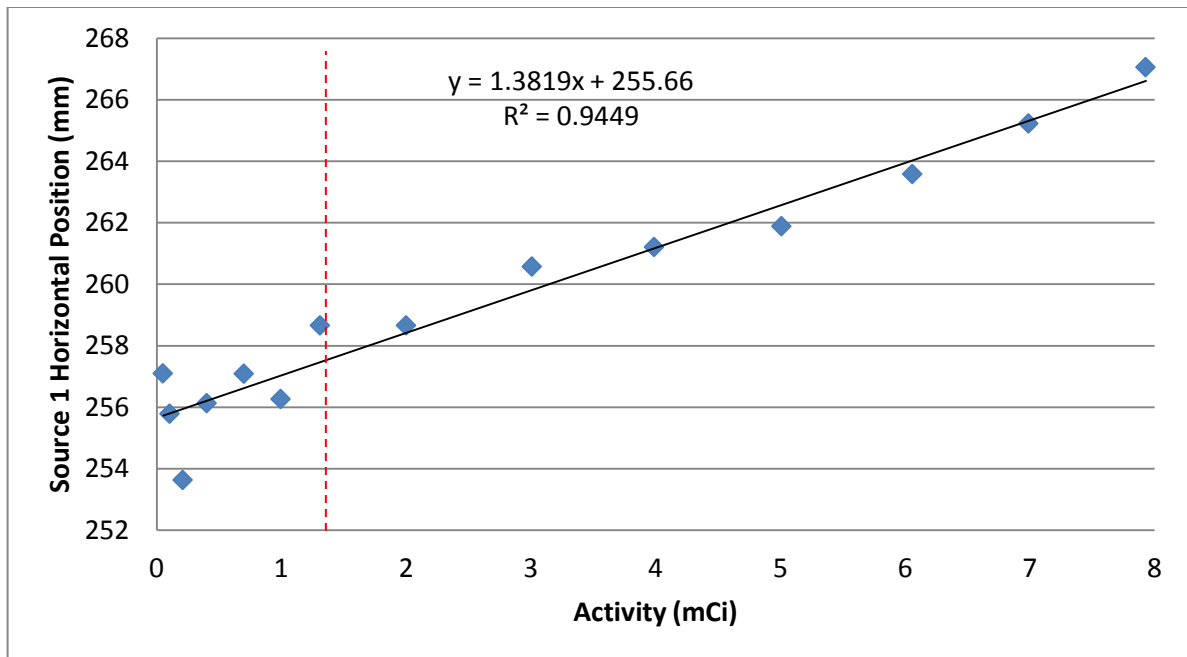


Fig. 6-10. The horizontal position of the center of mass of source 1 plotted against activity. As the total activity increases, the center of mass of source 1 shifts closer to source 2. The dashed line indicates the activity at which the MCR occurred.

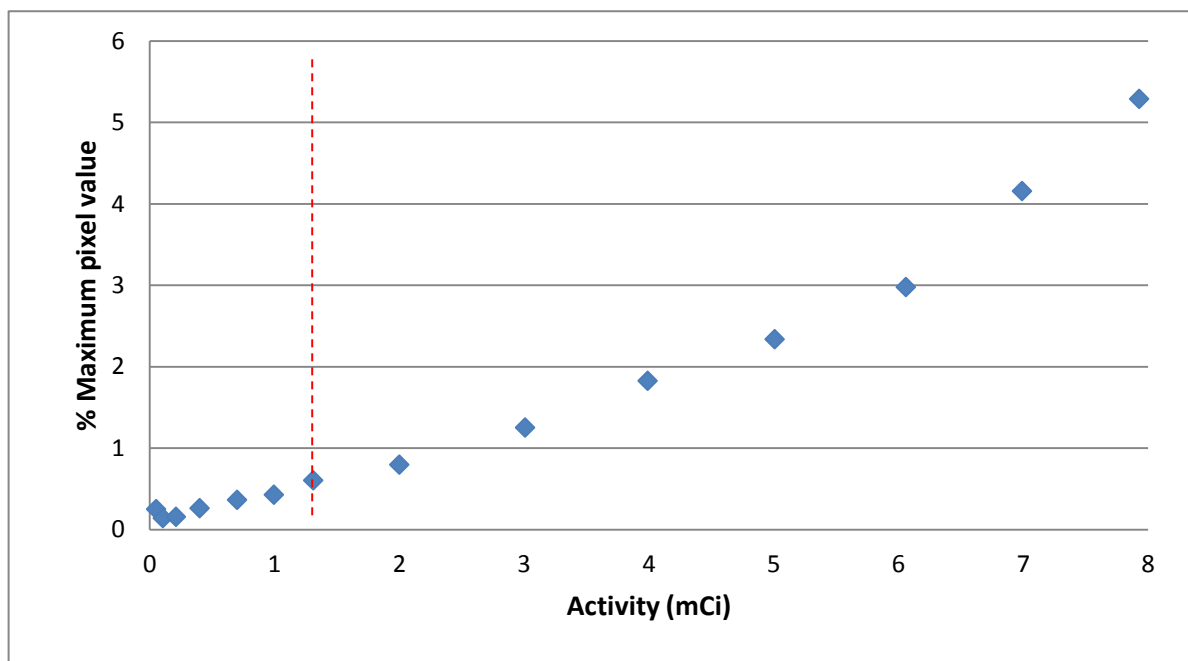


Fig. 6-11. The ratio of the maximum pixel value in the central ROI to the maximum pixel value in the entire image is plotted against the total activity. The dashed line indicates the activity at which the MCR occurred.

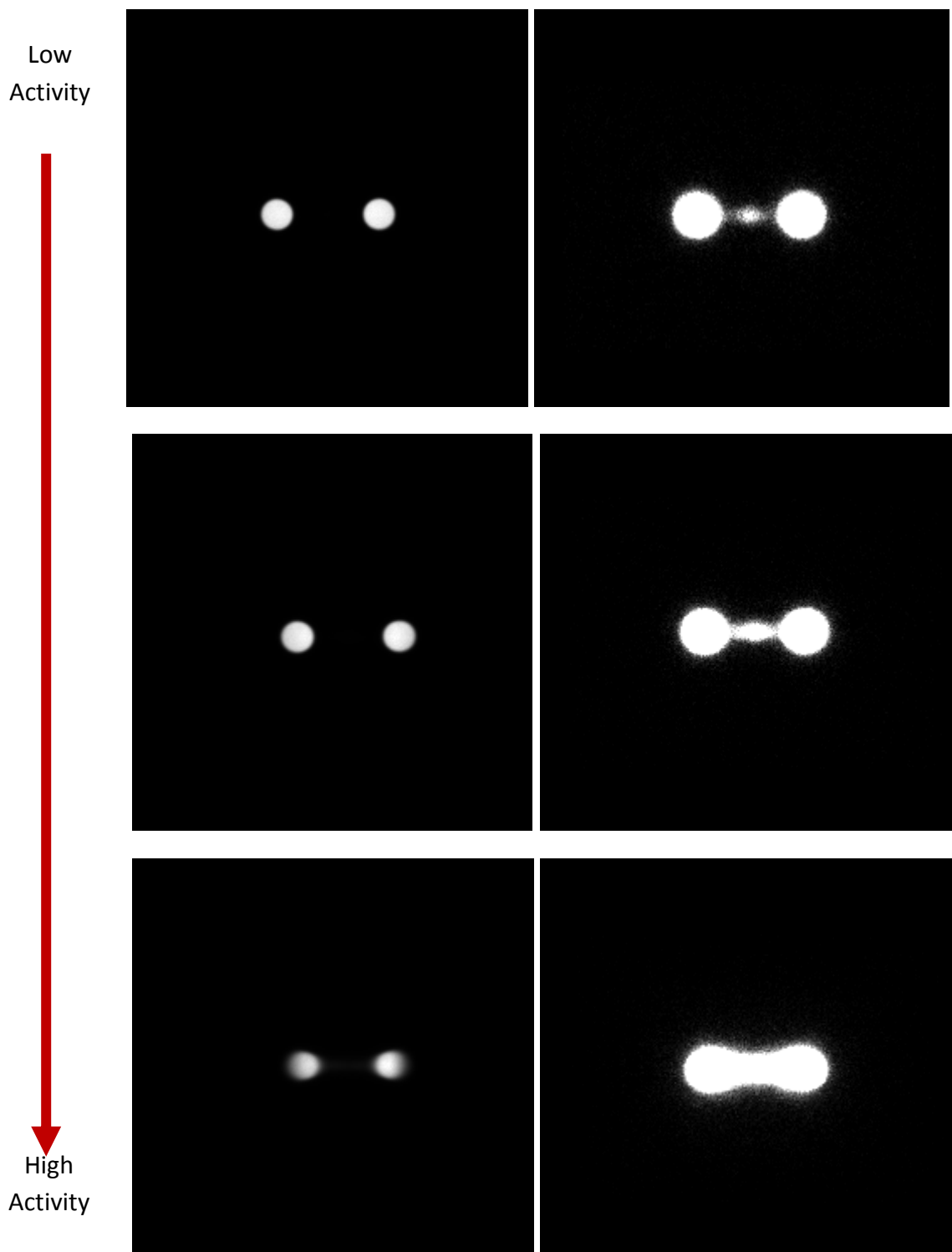


Fig. 6-12. Images of two sources used to evaluate image distorting effects of high count rates. Images in the left column are displayed at brightness and contrast settings typical for clinical imaging and illustrate the shift of the center of mass of the sources as activity increases. The right column displays the same images as on the left but viewed with low contrast, illustrating the mispositioning effects of high count rate.



## **7. DISCUSSION**

### **7.1 CRP of modern gamma cameras**

It has been observed that the CRP curves of the three modern gamma camera models investigated do not follow the PDM at all count rates. However, good agreement with the PDM was observed up to reasonably high input count rates (300-400 kcps, OW), beyond which these systems deviated substantially from the PDM. Owing to this behavior, the observed MCR for these cameras fell well below the predicted MCR assuming the PDM. As a result, MCR can not be directly related to  $\tau$  via Eqn. 2-8 for these cameras. Because MCR for these systems cannot be directly related to count rate losses, it does not provide an adequate metric for evaluating CRP. Since routine clinical imaging is always performed in the paralyzable portion of the CRP curve,  $\tau$ , estimated for this portion of the curve, is a better indicator of clinical CRP and is recommended for use in the dead time correction of observed count rates.

### **7.2 Comparison of Rates and Counts methods for analyzing Decay method data**

While it was observed that estimates of  $\tau$  determined using the Rates method and the Counts method were highly correlated, a small but significant bias was detected. Estimates of  $\tau$  using the Rates method were found to be greater than those using the Counts method by 0.029  $\mu$ s on average, corresponding to only ~6% of the value of  $\tau$  that is typical of these systems when using an open window. Estimates of the input count rate and the background used in the Rates method were found to be consistent with the predicted values from the Counts method (Table 3-3), suggesting that the assumption of minimal losses at low count

rates ( $<4$  kcps) used to estimate input count rate and correction for the background in the Rates method was reasonable. The true values of  $\tau$  for these gamma cameras are not known. In addition, the two methods yield highly correlated estimates with only a small bias; therefore, there is no strong justification to claim that one method provides a more accurate estimate than the other. Because the Counts method does not base estimates of input count rate on the lowest count rate data point or require explicit background correction, it may be possible to reduce the total time required for the data acquisition. This offers it a practical advantage over the Rates method.

### **7.3 Specific concerns regarding implementation of the Dual Source Method**

For routine quality control purposes, it is important to perform the Dual Source method in a manner that is repeatable (i.e., the consistent use of identical energy windows and spectral conditions). Additionally, the dependences of the Dual Source method on source activity ratio and count rate require that attention be paid to the activities used. It was observed that if the ratio of the individual source activity to the total activity is maintained between 40% and 60%,  $\tau$  can be expected to be within 5% of its value when the sources are of exactly equal activity. If the sources' activities are maintained between 45% and 55% of the total activity, this can be reduced to approximately 1%. Also, the count rate dependence of estimates of  $\tau$  using the Dual Source method requires that the total activity be consistent and that  $R_{12}$  fall within the paralyzable portion of the CRP curve (from about 35% to 95% of MCR for a Siemens Symbia). It should be noted that the observed count rate dependence (Fig. 4-2) is specific to the gamma camera on which it was tested (Siemens Symbia). Adams *et al.* observed that this dependence varied significantly among several earlier generation

models.<sup>3</sup> Given these observations, Dual Source measurements intended to estimate  $\tau$  should be performed with an activity such that  $R_{12}$  is near the highest count rate that falls within the paralyzable portion of the CRP curve without reaching the non-paralyzable portion.

#### **7.4 Comparison of Decay method and Dual Source method for evaluating CRP**

The estimates of  $\tau$  determined using the Decay method and the Dual Source method were found to be highly correlated with no statistically significant difference between them when  $R_{12}$  was maintained at about 95% of MCR. However, a single data point at  $\tau$  equal to approximately  $10\mu\text{s}$  obtained using a 2% energy window was observed to have a much greater difference in  $\tau$  ( $>2\mu\text{s}$ ) than the rest of the data set (Fig. 5-2). Small shifts in the energy spectrum can occur as a result of daily peaking of the system and due to different count rates ( $R_1$  and  $R_2$  vs.  $R_{12}$ ) used for the Dual Source method. These shifts can have a substantial effect on measurements made using a narrow energy window such as the 2% energy window measurement that produced this data point. It is suspected that this data point is an outlier, although it was not excluded from the Bland-Altman analysis.

Because  $\tau$  is an appropriate metric for evaluating CRP, the Dual Source method can be used for routine quality control. Given the convenience with which the Dual Source method can be performed and its excellent agreement with the results of the Decay method, the Dual Source method is ideal for obtaining estimates of  $\tau$  for the paralyzable portion of the CRP curve. For both methods, estimates of  $\tau$  may vary greatly with the ratio of counts in the energy window to the total counts. Effective energy has a smaller but not insignificant effect on estimates of  $\tau$  with the difference between the AIR and NEMA scatter conditions being less than 5% when using an OW. Therefore, it is imperative to use consistent energy

windows and scatter conditions when performing CRP testing in order to be able to evaluate changes in performance.

## **7.5 Comparison and Comments on Manufacturer Specification**

This work has demonstrated that a direct comparison to the manufacturer's specifications requires identical energy window and spectral conditions during CRP measurement. For the Symbia, Brightview, and Millenium gamma cameras, the manufacturer has provided the MCR as a performance specification observed (310 kcps, 350 kcps, and 220 kcps respectively) that is measured in accordance with NEMA recommendations. Both the Symbia and Millenium cameras were evaluated under similar conditions, resulting in MCR measurements of 240 kcps and 294 kcps respectively. A separate evaluation of Symbia dead time using the Dual Source method (AAPM Report 6) yielded  $\tau$  values of 1.424  $\mu$ s and 1.374  $\mu$ s for 3/8 in. and 5/8 in. crystals respectively.<sup>1</sup> Variations in the incident spectrum and consequently the ratio of the photopeak window counts to the total counts can have a substantial effect on the observed counts. Therefore, a direct comparison of MCR or  $\tau$  with other experiments or with a manufacturer's specifications is challenging.

For the purposes of acceptance testing, it may be beneficial for the manufacturers to provide specifications that are measured in a manner such that variation in the experimental set up does not lead to large fluctuations in the result. To address this issue, performance metrics (either MCR or  $\tau$ ) may be evaluated using an OW. It has been shown that the effects of spectral variations are mitigated when counts are observed across the entire spectrum. Additionally, since the MCR observed for the modern cameras tested cannot be directly

related to count rate losses, MCR has become less valuable as a performance metric. As a result,  $\tau$ , estimated for the paralyzable portion of the CRP curve using an OW, and the maximum paralyzable count rate may be more appropriate metrics for comparison to the manufacturer's specifications. Additionally, while an observed count rate at 20% loss has routinely been provided by some manufacturers, its inclusion as a performance specification is redundant if  $\tau$  is specified.

## **7.6 Guidelines for acceptance and annual CRP testing**

Because the CRP varies among different gamma camera models, it is our recommendation that CRP be evaluated using the Decay method during acceptance testing of a new camera to determine  $\tau$ , MCR, and the corresponding input count rate and source activity at which the MCR occurs. Placing the source or sources at 5 FOV from an uncollimated detector is a common testing geometry and a source holder can be easily constructed to maintain reproducibility. Additionally, an energy window should be selected for data acquisition. While theoretically an OW would be ideal for this purpose assuming that it was used by the manufacturer to determine performance specifications, the photopeak window defined by the manufacturer for Tc-99m (15 or 20%) is acceptable for this purpose. At this time, a reproducible testing geometry, energy window, and scatter conditions should be identified and all further tests should be performed in the same manner. Care should be taken to ensure low and stable background conditions during data acquisition. If the Decay data are to be analyzed via the Rates method then the last measurement with low source activity should be acquired at low count rates and a final background measurement should

be performed after the source has been removed. Following Decay method acquisition the data may be analyzed using either the Rates or Counts method to determine both  $\tau$  for the paralyzable portion of the CRP curve and the MCR at which the system agrees with the PDM. Additionally, the Dual Source method should be performed utilizing the same geometry, scatter conditions and energy windows as the Decay method (i.e., sources placed at 5 FOV, uncollimated detectors, and no additional scattering material). The total activity should be selected such that it results in count rates roughly between 90% and 95% of the MCR but within the paralyzable region of the CRP curve. Owing to the relatively high count rates used, acquisition times may be kept short and correction for radioactive decay may be ignored. A background measurement, followed by measurements of source 1 only, sources 1 and 2, source 2 only, and a second background should be performed. Estimates of  $\tau$  may be obtained through the use of Eqn. 2-10. Future evaluations of CRP (e.g. annual testing) may be performed using the Dual Source method alone if one ensures the consistent use of testing geometry, scatter conditions, energy windows, and activities.

## **7.7 Effects of count rate on common gamma camera performance metrics**

All measures of image uniformity were observed to degrade with increases in input count rate. However, only UFOV INT uniformity was observed to have a statistically significant non-zero slope for the regression performed on the paralyzable portion of the CRP curve. Also, the maximum values of percentage uniformity (Table 6.1) for this range fell below the quality assurance thresholds used at M.D. Anderson (UFOV INT  $\leq 6.5$ , UFOV DIFF  $\leq 3.5$ , CFOV INT  $\leq 5.5$ , CFOV DIFF  $\leq 3.5$ ) for a 10 million count intrinsic Tc-99m uniformity image. As indicated by the slopes of the regression lines (Figs. 6-5 A-D),

increases in count rate led to a more substantial loss in uniformity for the UFOV than the CFOV across the entire range of activities used. While the dependence of uniformity on activity and hence input count rate was observed to be statistically non-zero across the entire range, the lack of significant dependence for all but UFOV INT uniformity for the paralyzable portion of the CRP curve and the relatively small magnitude of the increase in this range indicates that loss of uniformity at higher count rates may not be a clinically significant concern.

Spatial resolution FWHM was observed to degrade linearly with input count rate. For the paralyzable portion of the CRP curve, the maximum value was 4.23 mm for the paralyzable portion of the CRP curve, exceeding an acceptable performance limit for intrinsic spatial resolution (4.1 mm) proposed as part of a separate evaluation<sup>13</sup>. Since the dependence of spatial resolution on activity was demonstrated to be statistically non-zero, and given the magnitude of the change for the paralyzable portion of the CRP curve, loss of spatial resolution may be a concern at high count rates. Further investigation is required to determine if these losses pose any clinically significant threat to image quality.

Energy resolution FWHM was observed to degrade linearly with input count rate. The range in energy resolution for the paralyzable portion of the CRP curve (11.02% to 13.57%) corresponds to a 3.91% loss of counts in a 15% photopeak window assuming that the peak is a perfect Gaussian function centered at 140 keV. The photopeak was observed to shift by approximately 2 keV in this range, resulting in an energy window that is not centered on the photopeak and an additional loss of counts of 2.66%. Data acquired as part of the measurements for Specific Aim I indicated that the observed MCR for a Symbia detector with the source in AIR using a 15% photopeak window approximately 204 kcps.

The corresponding input count rate was 289 kcps, demonstrating a loss of 29.4% at the MCR. This implies that the effects of count rate on energy resolution and photopeak energy result in approximately 1/5 of the total counts lost at the MCR. In the future, acquisition of data in list mode may allow for real-time monitoring of the shape and energy of the photopeak. It is possible that the energy windows used following a list mode acquisition could be tailored to the data in such a way as to compensate for these losses.

When evaluating the distortion of images produced at high count rates, two distinct effects were apparent. The first effect was a shifting and misshaping of the activity distribution of the sources as activity increased (see Fig.6-11). Based on the linear fit, the center of mass of the activity distribution of source 1 shifted approximately 2 mm over the paralyzable portion of the CRP curve. At clinical count rates, this shift would likely be much less than 1 mm, indicating that this effect is not clinically significant. It should be noted that this shift may be dependent on the distance between the sources. While misshaping of the activity distribution was visible at count rates well beyond the MCR, this effect was not apparent for the paralyzable portion of the CRP curve. The second effect was the appearance of counts located directly between the two sources. As illustrated in Fig. 6-11, the percentage of counts located between the activity distributions of the two sources relative to the rest of the image increased as count rate increased. While this effect is clearly visible when the images are viewed with a narrow grayscale window, the effect is not noticeable under clinical viewing conditions. Additionally, the maximum pixel value in the central ROI was always less than 1% of the maximum pixel value for the entire image for the paralyzable portion of the CRP curve.



While high count rate has been observed to affect uniformity, spatial resolution, and energy resolution, and has been observed to lead to image distortion effects, the clinical significance of these effects appears to be minimal when count rates are restricted to the paralyzable portion of the CRP curve. Typical clinical studies rarely approach the upper end of the paralyzable region and therefore it is unlikely that the effects of high count rates will have a substantial impact on image quality. It should be noted that these investigations were preliminary and that more thorough evaluation of the effects of count rate losses, especially the dependence on the spatial activity distribution, is necessary to fully characterize these phenomena. Additionally, the effects of high count rates on image contrast, particularly in the presence of background radiation, should be evaluated. However, the results of these investigations seem to indicate that correction for count rate losses in both planar and SPECT images should primarily focus on restoring correct pixel values across the image and not on redistribution of the measured signal.

## **7.8 Approaches for dead time corrections of SPECT and planar images**

In routine clinical practice, individual frames for SPECT or planar imaging are acquired with specific photopeak energy window definitions. Therefore, in order to correct the observed counts for dead time losses, an estimate of  $\tau$  for that specific photopeak energy window definition is needed. This work has demonstrated that  $\tau$  varies with both the ratio of counts in the photopeak window to the total counts and the effective energy. In the (likely) scenario where patient imaging and dead time measurements conditions are not identical, a correction to the measured estimate of  $\tau$  would be necessary. By varying the dead time measurement conditions, as was done in this work, the variation in  $\tau$  with the effective

energy and ratio of counts in the photopeak window to the total counts can be characterized. In theory, a look-up table of  $\tau$  for the photopeak window may be constructed based on the ratio of counts in the photopeak window to the total counts and the effective energy. Next, the actual effective energy and ratio of counts in the photopeak window to the total counts of the image frame to be corrected would also need to be determined. If the image frame can be acquired in list mode, this information will be readily obtainable. On the basis of this information, the appropriate estimate of  $\tau$  (from the look-up table) for dead time correction can be chosen.

If we assume that count rate losses occur uniformly across the field of view (which is not necessarily true for multi-zone architecture<sup>6</sup>), we can estimate the input count rate for a pixel by multiplying the observed count rate for that pixel by the ratio of the input count rate for the frame (using Eqn. 2-7 and the  $\tau$  determined for the frame in question) to the observed count rate for that frame. Such a correction methodology does not account for the effects of count rate loss on uniformity, resolution, and image distorting effects.

It is important to note that the dependence of  $\tau$  on the ratio of the counts in the photopeak window to the total counts has a substantially greater clinical effect than does the dependence of  $\tau$  on effective energy. Based on a preliminary investigation of Tc-99m bone scan spectra, the typical ratio of photopeak window counts to total counts is approximately  $30 \pm 10\%$ . Over this range, estimates of  $\tau$  vary between approximately  $3.8 \mu\text{s}$  and  $1.4 \mu\text{s}$  based on the functional form derived in section 3.3.4. For an input count rate of 20 kcps, these values correspond to observed count rates of 18.5 and 19.4 kcps respectively ( $\Delta \approx 5\%$ ). The typical effective energy for these spectra was approximately  $100 \pm 5 \text{ keV}$ . Across the entire range of energies tested (87.3 keV to 181.6 keV), the estimates of  $\tau$  varied only

between approximately  $0.55\ \mu\text{s}$  and  $0.35\ \mu\text{s}$  for the OW. For an input count rate of 20 kcps, these values correspond to observed count rates of 19.8 and 19.9 kcps, respectively ( $\Delta < 0.5\%$ ).

## 8. CONCLUSION

The hypothesis of this project was that the count rate performance of modern Anger type gamma cameras follows the PDM only up to a cutoff input count rate, below which the system dead time can be estimated using either the Decay or Dual Source methods. The CRP curves for three modern gamma camera models were demonstrated to agree with the PDM at lower count rates but to deviate substantially from it at higher input count rates, confirming the first part of the hypothesis. The Decay method and the Dual Source method for estimating  $\tau$  for the paralyzable portion of the CRP curve were investigated. A new method to analyze decay data using the measured counts (Counts method) was presented and shown to be consistent with the conventional Rates method. Estimates of  $\tau$  using the Decay method and the Dual Source method were compared, showing no statistically significant difference and confirming the second part of the hypothesis. The estimates of  $\tau$  depended on the ratio of counts in the photopeak window to the total counts and on the effective energy of the input spectrum. Also, the estimates of  $\tau$  using the Dual Source method were observed to vary as a quadratic function with the ratio of the single source to combined source activities and linearly with total activity used across a large range. A preliminary investigation was performed to observe the effects of count rate on several gamma camera performance metrics. On the basis of these investigations, guidelines have been provided for CRP testing in a clinical setting and a possible method for the correction of count rate losses for clinical images has been proposed.

## 9. FUTURE WORK

This work evaluated the CRP of three modern gamma cameras. However, there are many models of gamma camera that are currently in clinical use that were not investigated. Future work includes characterizing the CRP curves for other models to determine if all or a portion of their CRP curves may be fit with the PDM. Also, because the Counts method for fitting Decay method data does not base an estimate of the input count rates on the lowest observed count rate, it is possible that the acquisition time required to perform the Decay method may be reduced while maintaining accurate estimates of  $\tau$  for the paralyzable portion of the CRP curve. Further experimentation should be performed to identify an ideal procedure for the performance of the Decay method that optimizes acquisition time, initial activity, and interval duration ultimately leading to a procedure that is feasible for a clinical environment.

It has been demonstrated that estimates of  $\tau$  using the Dual Source method depend on the input count rate and that this dependence is gamma camera specific.<sup>3</sup> This work has characterized this dependence only for Siemens Symbia cameras. To utilize this method to estimate  $\tau$  for other models, it is necessary to investigate this dependence for the system in question to determine the range of activities with which  $\tau$  may be estimated consistently and accurately.

This work has made claims regarding the clinical significance of the effects of count rate losses on gamma camera performance. However, the experiments performed were preliminary in nature and a more thorough investigation is required to fully characterize these effects for both Symbia gamma cameras and other models. In particular, any

dependence of these effects on more complex spatial activity distributions should be tested. Also, the effects of the count rate on image contrast should be investigated. Finally, a comprehensive investigation regarding the effects of count rate on SPECT imaging should be performed.

This work has proposed a method for correcting count rate losses. To implement this method, a look-up table of  $\tau$  based on the ratio of the counts in the photopeak window to the total counts across the spectrum and the effective spectral energy must be constructed. The proposed method relies on the assumption that count rate losses as a fraction of pixel value are constant across an entire image frame regardless of the activity distribution. This assumption remains to be validated. If true, however, a study should be performed using the suggested look-up table to evaluate if count rate losses for individual SPECT frames can be accurately corrected as described. In the future, list mode data acquisition may become a reality for SPECT imaging, providing the information necessary for the correction of count rate losses for each individual frame.

## 10. BIBLIOGRAPHY

1. “Nuclear medicine/PET accreditation program requirements”, American College of Radiology (ACR), 2 Aug 2012, <http://www.acr.org/Quality-Safety/Accreditation/Nuclear-Med-PET>, Accessed 14 Aug 2012
2. “Performance measurement of gamma cameras," NEMA Standards Publication No. NU1-2007, (National Electrical Manufacturers Association, Washington, DC, 2007).
3. R. Adams, G.J. Hine, C.D. Zimmerman, “Deadtime measurements in scintillation cameras under scatter conditions simulating quantitative nuclear cardiology,” *J. Nucl. Med.* **19**, 538-544, (1978).
4. American Association of Physicists in Medicine (AAPM) Report No. 6, “Scintillation camera acceptance testing and performance evaluation,” (AAPM, College Park, MD, 1980) [www.aapm.org](http://www.aapm.org).
5. J.A. Sorenson, “Deadtime characteristics of Anger cameras,” *J. Nucl. Med.* **16**, 284-288, (1975).
6. T.W. Woldemichael, “Modeling of scintillation cameras with multi-zone architecture and pileup prevention circuitry,” *IEEE Transactions on Nuclear Science*, **54**, 690-698 (2007).
7. “Performance measurements of scintillation cameras,” NEMA Standards Publication No. NU 1-1986 (National Electrical Manufacturers Association, Washington, DC, 1986).
8. S. Cherry, J. Sorenson, and M. Phelps. Physics in Nuclear Medicine. 3<sup>rd</sup> Ed. (Saunders, Philadelphia, PA, 2003).
9. G. F. Knoll. Radiation Detection and Measurement. 4<sup>th</sup> Ed. (Wiley, Hoboken, NJ, 2000)

10. R. Adams, "Suggested revision of NEMA standards," *J. Nucl. Med.* **25**, 814-816 (1984).
11. E.M. Geldenhuys, M. G. Lotter, P. C. Minnaar, "A new approach to NEMA scintillation camera count rate curve determination," *J. Nucl. Med.* **29**, 538-541, (1988).
12. J. M. Bland and D. G. Altman, "Statistical methods for assessing agreement between two methods of clinical measurement," *Lancet* **1** (8476), 307–310 (1987).
13. S. C. Kappadath, W.D. Erwin, and R.E. Wendt III, "Observed intercamera variability in clinically relevant performance characteristics for Siemens Symbia gamma cameras," *JACMP*. **7**,4, (2006)
14. CRC, Standard Mathematical Tables, 26<sup>th</sup> Ed. 1981/82. CRC Press, Boca Raton, Florida, p. 330, entry #522.



## 11. APPENDIX

### Derivation of the Counts Method Model

The derivation of an expression representing the mean counts observed during a counting interval from  $t_0$  to  $t_1$  and accounting for source decay is as follows:

For a paralyzable detector exposed to a decaying radioactive source, the mean observed count rate ( $m$ ) may be related to the mean input count rate ( $n$ ) via the following expression:

$$m = ne^{-n\tau} \quad (A1)$$

where  $\tau$  represents the system dead time. The mean input count rate is a function of both the background count rate ( $b$ ) and the decay of the source and can be represented with the following equation:

$$n = b + A_0 e^{-\lambda t} \quad (A2)$$

where  $\lambda$  is the decay constant of the source,  $t$  is time, and  $A_0$  is the input count rate at  $t = 0$ . Substitution of Eqn. A2 in Eqn. A1 yields

$$m = (b + A_0 e^{-\lambda t})e^{-(b + A_0 e^{-\lambda t})\tau} \quad (A3)$$

The mean counts observed during a counting interval from  $t_0$  to  $t_1$  ( $M_{(t_0, t_1)}$ ) may be determined by integrating the mean observed count rate over the time interval in question.

$$M_{(t_0, t_1)} = \int_{t_0}^{t_1} m dt \quad (A4)$$

Substitution of Eqn. A3 in Eqn. A4 yields

$$M_{(t_0, t_1)} = \int_{t_0}^{t_1} (b + A_o e^{-\lambda t}) * e^{-(b+A_o e^{-\lambda t})\tau} dt \quad (\text{A5})$$

assuming that the background count rate is independent of time. This expression may be simplified via distribution to yield

$$M_{(t_0, t_1)} = \int_{t_0}^{t_1} b e^{-(b+A_o e^{-\lambda t})\tau} dt + \int_{t_0}^{t_1} (A_o e^{-\lambda t}) e^{-(b+A_o e^{-\lambda t})\tau} dt \quad (\text{A6})$$

The second term in this expression has a closed form solution<sup>14</sup>. As a result, Eqn. A6 may be further simplified as shown

$$\begin{aligned} M_{(t_0, t_1)} &= \int_{t_0}^{t_1} b e^{-(b+A_o e^{-\lambda t})\tau} dt + \int_{t_0}^{t_1} (A_o e^{-\lambda t}) e^{-(b+A_o e^{-\lambda t})\tau} dt \\ &= b e^{-b\tau} \int_{t_0}^{t_1} e^{-(A_o e^{-\lambda t})\tau} dt + \frac{e^{-b\tau}}{\lambda\tau} e^{-(A_o \tau e^{-\lambda t})} \Big|_{t_0}^{t_1} \\ &= b e^{-b\tau} \int_{t_0}^{t_1} e^{-(A_o e^{-\lambda t})\tau} dt + \frac{e^{-b\tau}}{\lambda\tau} (e^{-(A_o \tau e^{-\lambda t_1})} - e^{-(A_o \tau e^{-\lambda t_0})}) \end{aligned} \quad (\text{A7})$$

To derive an expression for the first term of Eqn. A7 a change of variables is performed as follows:

$$y = A_o e^{-\lambda t} \tau$$

$$\text{Then } \frac{dy}{dt} = A_o e^{-\lambda t} (-\tau\lambda) = -\lambda * y \text{ and } dt = -\frac{dy}{y\lambda}$$

The integral from the first term of Eqn. A7 can be represented as a function of y

$$\begin{aligned} \int_{t_0}^{t_1} e^{-(A_o e^{-\lambda t})\tau} dt &= \int_{t_0}^{t_1} e^{-y} dt \\ &= \int_{y_0}^{y_1} e^{-y} * \frac{-1}{\lambda y} dy \end{aligned}$$

$$= \frac{-1}{\lambda} \int_{y_0}^{y_1} \frac{e^{-y}}{y} dy \quad (\text{A8})$$

where  $y_0 = A_o e^{-\lambda t_0} \tau$  and  $y_1 = A_o e^{-\lambda t_1} \tau$ . Eq. (A8) may be expanded via Taylor Series<sup>14</sup> yielding

$$\begin{aligned} \frac{-1}{\lambda} \int_{y_0}^{y_1} \frac{e^{-y}}{y} dy &= \frac{-1}{\lambda} \left[ \ln y - y + \frac{y^2}{4} + \frac{y^3}{18} + \frac{y^4}{96} + \dots \right]_{y_0}^{y_1} \\ &= \frac{-1}{\lambda} \left[ \ln y_1 - \ln y_0 - (y_1 - y_0) + \frac{y_1^2 - y_0^2}{4} + \frac{y_1^3 - y_0^3}{18} + \frac{y_1^4 - y_0^4}{96} + \dots \right] \\ &= \frac{-1}{\lambda} \ln \left( \frac{y_1}{y_0} \right) - (y_1 - y_0) + \frac{y_1^2 - y_0^2}{4} + \frac{y_1^3 - y_0^3}{18} + \frac{y_1^4 - y_0^4}{96} + \dots \end{aligned} \quad (\text{A9})$$

Substituting  $y_0$  and  $y_1$  into Eqn. A9 results in

$$\begin{aligned} \frac{-1}{\lambda} \int_{y_0}^{y_1} \frac{e^{-y}}{y} dy &= \frac{-1}{\lambda} \left[ \ln \frac{A_o e^{-\lambda t_1} \tau}{A_o e^{-\lambda t_0} \tau} - (A_o e^{-\lambda t_1} \tau - A_o e^{-\lambda t_0} \tau) + \frac{\left( (A_o e^{-\lambda t_1} \tau) \right)^2 - \left( (A_o e^{-\lambda t_0} \tau) \right)^2}{4} \right. \\ &\quad \left. - \frac{\left( (A_o e^{-\lambda t_1} \tau) \right)^3 - \left( (A_o e^{-\lambda t_0} \tau) \right)^3}{18} + \frac{\left( (A_o e^{-\lambda t_1} \tau) \right)^4 - \left( (A_o e^{-\lambda t_0} \tau) \right)^4}{96} + \dots \right] \\ &= (t_1 - t_0) - \frac{1}{\lambda} \left[ -(A_o \tau) (e^{-\lambda t_1} - e^{-\lambda t_0}) + \frac{(A_o \tau)^2}{4} ((e^{-\lambda t_1})^2 - (e^{-\lambda t_0})^2) \right. \\ &\quad \left. - \frac{(A_o \tau)^3}{18} ((e^{-\lambda t_1})^3 - (e^{-\lambda t_0})^3) + \frac{(A_o \tau)^4}{96} ((e^{-\lambda t_1})^4 - (e^{-\lambda t_0})^4) + \dots \right] \end{aligned} \quad (\text{A10})$$

Because  $t_1$  and  $t_0$  are at the most 16 minutes apart, the counting intervals are short relative to the half-life of the source and  $\frac{e^{-\lambda t_1}}{e^{-\lambda t_0}}$  is  $\sim 3\%$ . The following simplifications were made:

$$(e^{-\lambda t_1})^k - (e^{-\lambda t_0})^k = (e^{-\lambda t_1} - e^{-\lambda t_0}) k e^{-(k-1)\lambda t_0'} \quad k=2,3,4,\dots \quad (\text{A11})$$

where 
$$e^{-\lambda t_1} + e^{-\lambda t_0} = 2e^{-\frac{\lambda(t_1+t_0)}{2}} = 2e^{-\lambda t'_0} \quad (\text{A12})$$

Substitution of Eqn. A11 into Eqn. A10 yields

$$\begin{aligned} \frac{-1}{\lambda} * \int_{y_0}^{y_1} \frac{e^{-y}}{y} dy &= t_1 - t_0 - \frac{1}{\lambda} [-(A_0\tau)(e^{-\lambda t_1} - e^{-\lambda t_0}) + \frac{(A_0\tau)^2}{4} ((e^{-\lambda t_1})^2 - (e^{-\lambda t_0})^2) \\ &\quad - \frac{(A_0\tau)^3}{18} ((e^{-\lambda t_1})^3 - (e^{-\lambda t_0})^3) + \frac{(A_0\tau)^4}{96} ((e^{-\lambda t_1})^4 - (e^{-\lambda t_0})^4) + \dots] \\ &= t_1 - t_0 + \left(\frac{A_0\tau}{\lambda}\right) (e^{-\lambda t_1} - e^{-\lambda t_0}) - \frac{(A_0\tau)^2}{2\lambda} (e^{-\lambda t_1} - e^{-\lambda t_0}) * e^{-\lambda t'_0} \\ &\quad + \frac{(A_0\tau)^3}{6} (e^{-\lambda t_1} - e^{-\lambda t_0}) * e^{-2\lambda t'_0} - \frac{(A_0\tau)^4}{24} (e^{-\lambda t_1} - e^{-\lambda t_0}) * e^{-3\lambda t'_0} + \dots \quad (\text{A13}) \end{aligned}$$

Eqn. A13 may be substituted for the integral of the first term of Eqn. A7 resulting in

$$\begin{aligned} M_{(t_0, t_1)} &= \frac{e^{-b\tau}}{\lambda\tau} \left( e^{-(A_0\tau e^{-\lambda t_1})} - e^{-(A_0\tau e^{-\lambda t_0})} \right) + b e^{-b\tau} (t_1 - t_0) \\ &\quad + \frac{A_0\tau}{\lambda} b e^{-b\tau} (e^{-\lambda t_1} - e^{-\lambda t_0}) * \left( 1 - \frac{A_0\tau}{2} e^{-\lambda t'_0} + \frac{(A_0\tau)^2}{6} e^{-2\lambda t'_0} - \frac{(A_0\tau)^3}{24} e^{-3\lambda t'_0} + \dots \right) \end{aligned}$$

The final expression for the counts observed during the counting interval from  $t_0$  to  $t_1$  accounting for radioactive decay and background count rate used in the Counts method is given by:

$$\begin{aligned} M_{(t_0, t_1)} &= \frac{e^{-b\tau}}{\lambda\tau} \left( e^{-(A_0\tau e^{-\lambda t_1})} - e^{-(A_0\tau e^{-\lambda t_0})} \right) + b e^{-b\tau} (t_1 - t_0) \\ &\quad + \frac{A_0\tau}{\lambda} b e^{-b\tau} (e^{-\lambda t_1} - e^{-\lambda t_0}) \left( 1 - \frac{A_0\tau}{2} e^{-\frac{\lambda(t_1+t_0)}{2}} + \frac{(A_0\tau)^2}{6} e^{-\lambda(t_1+t_0)} - \frac{(A_0\tau)^3}{24} e^{-\frac{3*\lambda(t_1+t_0)}{2}} \right) \quad (\text{A13}) \end{aligned}$$

This series was observed to converge rapidly so additional terms beyond those shown in Eqn. A13 were not included for use in the Counts method.

## **Vita**

Michael Silosky was born in Downers Grove, Illinois on September 10, 1981 to Steve and Janet Silosky. He is married to Joanna Silosky and has three children, Hank, Lynne, and Mark. He entered the Army National Guard in 1998 and attended the United States Military Academy at West Point, New York for 2 years. He graduated from the University of Illinois at Urbana-Champaign with a B.S. in Physics in December 2005. In July, 2006 he began work for The University of Texas M.D. Anderson Cancer Center as a Physics Technologist in the department of Imaging Physics. He has remained employed in this position part time after entering the University of Texas Health Science Center at Houston Graduate School of Biomedical Sciences in May 2011.

Permanent address:

13614 Salisbury Dr.

Sugar Land, TX 77498